the genes/loci responsible for the phenotype established. In the near future, with advances in gene-targeting technologies by using ES or iPS cells capable of germ-line transmission, in combination with the nuclear transfer technique, more precise manipulation of the rabbit genome may also be available. Since the lesion composition and severity of coronary lesions differ even in WHHLMI rabbits, despite no difference in the serum cholesterol levels, it will be important to explore marker proteins and/or risk factors affecting coronary lesions. Once markers and risk factors relating to vulnerable coronary atheromas are found, the mechanism of cardiovascular events may be clarified. Such findings would contribute to the development of new clinical diagnostics and thence to the prevention of cardiovascular events.

In conclusion, selecting appropriate animal model is important in translational research. WHHL and WHHLMI rabbits have contributed to development of hypocholesterolemic and antiatherosclerotic compounds and medical devices, such as imaging technologies for atherosclerosis, and diagnostic techniques for acute coronary syndromes, in addition to elucidation of the mechanisms of atherogenesis and coronary plaque rupture. These studies are helpful for progression of therapeutics.

Acknowledgments

This work was supported in part by a Grant-in-Research on Biological Resource and Animal Models for Drug Development from the Ministry of Health and Labor in Japan and a research grant from the Ministry of Education, Culture, Science and Technology of Japan. The authors thank Sankyo Co., Ltd., Tokyo, Japan; Takeda Pharmaceutical Co., Ltd., Osaka, Japan; Daiich-Sankyo Co., Ltd., Tokyo, Japan; Shionogi & Co. Ltd, Osaka, Japan; Taisho Pharmaceutical Co. Ltd., Tokyo, Japan; Otsuka Pharmaceutical Co. Ltd., Tokushima, Japan, Banyu Pharmaceutical Co. Ltd., Tokyo, Japan; Nippon Shinyaku Co. Ltd., Osaka, Japan for their support in the maintenance of the WHHL or WHHLMI rabbit strain from 1980 to 2010.

References

[1] World Health Organization, *The World Health Report 2002—Reducing Risks, Promoting Healthy Life: Statistical Annex*, World Health Organization, Geneva, Switzerland, 2002.

[2] T. Teramoto, J. Sasaki, H. Ueshima et al., "Executive summary of Japan Atherosclerosis Society (JAS) guideline for diagnosis and prevention of atherosclerotic cardiovascular diseases for Japanese," *Journal of Atherosclerosis and Thrombosis*, vol. 14, no. 2, pp. 45–50, 2007.

[3] S. Yusuf and S. Anand, "Cost of prevention: the case of lipid lowering," *Circulation*, vol. 93, no. 10, pp. 1774–1776, 1996.

[4] A. Endo, M. Kuroda, and Y. Tsujita, "ML 236A, ML 236B, and ML 236C, new inhibitors of cholesterogenesis produced by Penicillium citrinum," *Journal of Antibiotics*, vol. 29, no. 12, pp. 1346–1348, 1976.

[5] Y. Tsujita, M. Kuroda, and Y. Shimada, "CS-514, a competitive inhibitor of 3-hydroxy-3-methylglutaryl coenzyme A reductase: tissue-selective inhibition of sterol synthesis and hypolipidemic effect on various animal species," *Biochimica et Biophysica Acta*, vol. 877, no. 1, pp. 50–60, 1986.

[6] Y. Watanabe, "Studies on characteristic of spontaneously hyperlipidemic rabbit and development of the strain with such property," *Bulletin of Azabu Veterinary College*, vol. 2, no. 1, pp. 99–124, 1977 (Japanese).

[7] T. V. Liew and K. K. Ray, "Intensive statin therapy in acute coronary syndromes," *Current Atherosclerosis Reports*, vol. 10, no. 2, pp. 158–163, 2008.

[8] M. Shiomi and T. Ito, "The Watanabe heritable hyperlipidemic (WHHL) rabbit, its characteristics and history of development: a tribute to the late Dr. Yoshio Watanabe," *Atherosclerosis*, vol. 207, no. 1, pp. 1–7, 2009.

[9] Y. Watanabe, T. Ito, and T. Kondo, "Breeding of a rabbit strain of hyperlipidemia and characteristic of these strain," *Experimental Animals*, vol. 26, no. 1, pp. 35–42, 1977 (Japanese).

[10] Y. Watanabe, "Serial inbreeding of rabbits with hereditary hyperlipidemia (WHHL-rabbit). Incidence and development of atherosclerosis and xanthoma," *Atherosclerosis*, vol. 36, no. 2, pp. 261–268, 1980.

[11] K. Tanzawa, Y. Shimada, and M. Kuroda, "WHHL-rabbit: a low density lipoprotein receptor-deficient animal model for familial hypercholesterolemia," *FEBS Letters*, vol. 118, no. 1, pp. 81–84, 1980.

[12] R. J. Havel, T. Kita, and L. Kotite, "Concentration and composition of lipoproteins in blood plasma of the WHHL rabbit. An animal model of human familial hypercholesterolemia," *Arteriosclerosis*, vol. 2, no. 6, pp. 467–474, 1982.

[13] T. Kita, M. Brown, D. W. Bilheimer, and J. L. Goldstein, "Delayed clearance of very low density and intermediate density lipoprotein with enhanced conversion to low density lipoprotein in WHHL rabbits," *Proceedings of the National Academy of Sciences of the United States of America*, vol. 79, no. 18, pp. 5693–5697, 1982.

[14] T. Kita, J. L. Goldstein, and M. S. Brown, "Hepatic uptake chylomicron remnants in WHHL rabbits: a mechanism genetically distinct from the low density lipoprotein receptor," *Proceedings of the National Academy of Sciences of the United States of America*, vol. 79, no. 11, pp. 3623–3627, 1982.

[15] J. M. Dietschy, T. Kita, and K. E. Suckling, "Cholesterol synthesis in vivo and in vitro in the WHHL rabbit, an animal with defective low density lipoprotein receptors," *Journal of Lipid Research*, vol. 24, no. 4, pp. 469–480, 1983.

[16] Y. Watanabe, T. Ito, and M. Shiomi, "The effect of selective breeding on the development of coronary atherosclerosis in WHHL rabbits. An animal model for familial hypercholesterolemia," *Atherosclerosis*, vol. 56, no. 1, pp. 71–79, 1985.

[17] M. Shiomi, T. Ito, M. Shiraishi, and Y. Watanabe, "Inheritability of atherosclerosis and the role of lipoproteins as risk factors in the development of atherosclerosis in WHHL rabbits: risk factors related to coronary atherosclerosis are different from those related to aortic atherosclerosis," *Atherosclerosis*, vol. 96, no. 1, pp. 43–52, 1992.

[18] M. Shiomi, T. Ito, S. Yamada, S. Kawashima, and J. Fan, "Development of an animal model for spontaneous myocardial infarction (WHHLMI rabbit)," *Arteriosclerosis, Thrombosis, and Vascular Biology*, vol. 23, no. 7, pp. 1239–1244, 2003.

[19] M. Shiomi and J. Fan, "Unstable coronary plaques and cardiac events in myocardial infarction-prone Watanabe heritable hyperlipidemic rabbits: questions and quandaries," *Current Opinion in Lipidology*, vol. 19, no. 6, pp. 631–636, 2008.

[20] M. Shiomi, T. Ito, T. Tsukada, T. Yata, and M. Ueda, "Cell compositions of coronary and aortic atherosclerotic lesions in WHHL rabbits differ: an immunohistochemical study,"

Arteriosclerosis and Thrombosis, vol. 14, no. 6, pp. 931–937, 1994.

[21] M. Shiomi, T. Ito, T. Fujioka, and Y. Tsujita, "Age-associated decrease in plasma cholesterol and changes in cholesterol metabolism in homozygous Watanabe heritable hyperlipidemic rabbits," *Metabolism*, vol. 49, no. 4, pp. 552–556, 2000.

[22] T. Ito, S. Yamada, and M. Shiomi, "Progression of coronary atherosclerosis relates to the onset myocardial infarction in an animal model of spontaneous myocardial infarction (WHHLMI rabbits)," *Experimental Animals*, vol. 53, no. 4, pp. 339–346, 2004.

[23] H. O. Mowri, S. Ohkuma, and T. Takano, "Monoclonal DLR1a/104G antibody recognizing peroxidized lipoproteins in atherosclerotic lesions," *Biochimica et Biophysica Acta*, vol. 963, no. 2, pp. 208–214, 1988.

[24] H. C. Boyd, A. M. Gown, G. Wolfbauer, and A. Chait, "Direct evidence for a protein recognized by a monoclonal antibody against oxidatively modified LDL in atherosclerotic lesions from a Watanabe heritable hyperlipidemic rabbit," *American Journal of Pathology*, vol. 135, no. 5, pp. 815–825, 1989.

[25] T. Kita, Y. Nagano, M. Yokode et al., "Probucol prevents the progression of atherosclerosis in Watanabe heritable hyperlipidemic rabbit, an animal model for familial hypercholesterolemia," *Proceedings of the National Academy of Sciences of the United States of America*, vol. 84, no. 16, pp. 5928–5931, 1987.

[26] T. E. Carew, D. C. Schwenke, and D. Steinberg, "Antiatherogenic effect of probucol unrelated to its hypocholesterolemic effect: evidence that antioxidants in vivo can selectively inhibit low density lipoprotein degradation in macrophage-rich fatty streaks and slow the progression of atherosclerosis in the Watanabe heritable hyperlipidemic rabbit," *Proceedings of the National Academy of Sciences of the United States of America*, vol. 84, no. 21, pp. 7725–7729, 1987.

[27] M. I. Cybulsky and M. A. Gimbrone Jr., "Endothelial expression of a mononuclear leukocyte adhesion molecule during atherogenesis," *Science*, vol. 251, no. 4995, pp. 788–791, 1991.

[28] L. M. Buja, T. Kuta, and J. L. Goldstein, "Cellular pathology of progressive atherosclerosis in the WHHL rabbit. An animal model of familial hypercholesterolemia," *Arteriosclerosis*, vol. 3, no. 1, pp. 87–101, 1983.

[29] M. E. Rosenfeld, T. Tsukada, A. M. Gown, and R. Ross, "Fatty streak initiation in Watanabe Heritable Hyperlipemic and comparably hypercholesterolemic fat-fed rabbits," *Arteriosclerosis*, vol. 7, no. 1, pp. 9–23, 1987.

[30] M. E. Rosenfeld, T. Tsukada, A. Chait, E. L. Bierman, A. M. Gown, and R. Ross, "Fatty streak expansion and maturation in Watanabe heritable hyperlipidemic and comparably hypercholesterolemic fat-fed rabbits," *Arteriosclerosis*, vol. 7, no. 1, pp. 24–34, 1987.

[31] T. Takano, K. Amanuma, J. Kimura, T. Kanaseki, and S. Ohkuma, "Involvement of macrophages in accumulation and elimination of cholesterol ester in atherosclerotic aorta," *Acta Histochemica et Cytochemica*, vol. 19, no. 1, pp. 135–143, 1986.

[32] T. Tsukada, M. Rosenfeld, R. Ross, and A. M. Gown, "Immunocytochemical analysis of cellular components in atherosclerotic lesions. Use of monoclonal antibodies with the Watanabe and fat-fed rabbit," *Arteriosclerosis*, vol. 6, no. 6, pp. 601–613, 1986.

[33] K. F. Kozarsky, D. K. Bonen, F. Giannoni, T. Funahashi, J. M. Wilson, and N. O. Davidson, "Hepatic expression of the catalytic subunit of the apolipoprotein B mRNA editing enzyme (apobec-1) ameliorates hypercholesterolemia in LDL receptor-deficient rabbits," *Human Gene Therapy*, vol. 7, no. 8, pp. 943–957, 1996.

[34] M. Nakamuta, S. Taniguchi, B. Y. Ishida, K. Kobayashi, and L. Chan, "Phenotype interaction of apobec-1 and CETP, LDLR, and ApoE gene expression in mice: role of ApoB mRNA editing in lipoprotein phenotype expression," *Arteriosclerosis, Thrombosis, and Vascular Biology*, vol. 18, no. 5, pp. 747–755, 1998.

[35] B. Perret, L. Mabile, L. Martinez, F. Tercé, R. Barbaras, and X. Collet, "Hepatic lipase: structure/function relationship, synthesis, and regulation," *Journal of Lipid Research*, vol. 43, no. 8, pp. 1163–1169, 2002.

[36] L. B. Agellon, A. Walsh, T. Hayek et al., "Reduced high density lipoprotein cholesterol in human cholesteryl ester transfer protein transgenic mice," *The Journal of Biological Chemistry*, vol. 266, no. 17, pp. 10796–10801, 1991.

[37] Y. Watanabe, T. Ito, and M. Saeki, "Hypolipidemic effects of CS-500 (ML-236B) in WHHL-rabbit, a heritable animal model for hyperlipidemia," *Atherosclerosis*, vol. 38, no. 1-2, pp. 27–31, 1981.

[38] M. Shiomi and T. Ito, "Pravastatin sodium, a competitive inhibitor of hepatic 3-hydroxy-3- methylglutaryl coenzyme a reductase, decreases the cholesterol content of newly secreted very-low-density lipoprotein in Watanabe heritable hyperlipidemic rabbits," *Metabolism*, vol. 43, no. 5, pp. 559–564, 1994.

[39] M. Kuroda, A. Matsumoto, H. Itakura et al., "Effects of pravastatin sodium alone and in combination with cholestyramine on hepatic, intestinal and adrenal low density lipoprotein receptors in homozygous Watanabe heritable hyperlipidemic rabbits," *Japanese Journal of Pharmacology*, vol. 59, no. 1, pp. 65–70, 1992.

[40] M. Shiomi, T. Ito, Y. Watanabe et al., "Suppression of established atherosclerosis and xanthomas in mature WHHL rabbits by keeping their serum cholesterol levels extremely low. Effect of pravastatin sodium in combination with cholestyramine," *Atherosclerosis*, vol. 83, no. 1, pp. 69–80, 1990.

[41] Y. Watanabe, T. Ito, M. Shiomi et al., "Preventive effect of pravastatin sodium, a potent inhibitor of 3-hydroxy-3-methylglutaryl coenzyme A reductase, on coronary atherosclerosis and xanthoma in WHHL rabbits," *Biochimica et Biophysica Acta*, vol. 960, no. 3, pp. 294–302, 1988.

[42] M. Shiomi, T. Ito, T. Tsukada et al., "Reduction of serum cholesterol levels alters lesional composition of atherosclerotic plaques: effect of pravastatin sodium on atherosclerosis in mature WHHL rabbits," *Arteriosclerosis, Thrombosis, and Vascular Biology*, vol. 15, no. 11, pp. 1938–1944, 1995.

[43] M. Shiomi and T. Ito, "Effect of cerivastatin sodium, a new inhibitor of HMG-CoA reductase, on plasma lipid levels, progression of atherosclerosis, and the lesional composition in the plaques of WHHL rabbits," *British Journal of Pharmacology*, vol. 126, no. 4, pp. 961–968, 1999.

[44] M. Shiomi, T. Ito, Y. Hirouchi, and M. Enomoto, "Fibromuscular cap composition is important for the stability of established atherosclerotic plaques in mature WHHL rabbits treated with statins," *Atherosclerosis*, vol. 157, no. 1, pp. 75–84, 2001.

[45] M. Shiomi, S. Yamada, and T. Ito, "Atheroma stabilizing effects of simvastatin due to depression of macrophages or lipid accumulation in the atheromatous plaques of coronary plaque-prone WHHL rabbits," *Atherosclerosis*, vol. 178, no. 2, pp. 287–294, 2005.

[46] H. Otake, J. Shite, T. Shinke et al., "Relation between plasma adiponectin, high-sensitivity C-reactive protein, and coronary plaque components in patients with acute coronary

syndrome," *American Journal of Cardiology*, vol. 101, no. 1, pp. 1–7, 2008.

[47] M. B. Pepys, M. Baltz, and K. Gomer, "Serum amyloid P-component is an acute-phase reactant in the mouse," *Nature*, vol. 278, no. 5701, pp. 259–261, 1979.

[48] J. Fan and T. Watanabe, "Transgenic rabbits as therapeutic protein bioreactors and human disease models," *Pharmacology and Therapeutics*, vol. 99, no. 3, pp. 261–282, 2003.

[49] G. Liu, J. B. Iden, K. Kovithavongs, R. Gulamhusein, H. J. Duff, and K. M. Kavanagh, "In vivo temporal and spatial distribution of depolarization and repolarization and the illusive murine T wave," *Journal of Physiology*, vol. 555, no. 1, pp. 267–279, 2004.

[50] B. London, "Cardiac arrhythmias: from (transgenic) mice to men," *Journal of Cardiovascular Electrophysiology*, vol. 12, no. 9, pp. 1089–1091, 2001.

[51] G. C. Ness, Z. Zhao, and R. K. Keller, "Effect of squalene synthase inhibition on the expression of hepatic cholesterol biosynthetic enzymes, LDL receptor, and cholesterol 7α hydroxylase," *Archives of Biochemistry and Biophysics*, vol. 311, no. 2, pp. 277–285, 1994.

[52] W. J. Schneider, M. S. Brown, and J. L. Goldstein, "Kinetic defects in the processing of the low density lipoprotein receptor in fibroblasts from WHHL rabbits and a family with familial hypercholesterolemia," *Molecular Biology & Medicine*, vol. 1, no. 3, pp. 353–367, 1983.

[53] M. T. R. Subbiah, R. L. Yunker, Z. Rymaszewski, B. A. Kottke, and L. K. Bale, "Cholestyramine treatment in early life of low-density lipoprotein receptor deficient Watanabe rabbits: decreased aortic cholesteryl ester accumulation and atherosclerosis in adult life," *Biochimica et Biophysica Acta*, vol. 920, no. 3, pp. 251–258, 1987.

[54] M. Shiomi and T. Ito, "MTP inhibitor decreases plasma cholesterol levels in LDL receptor-deficient WHHL rabbits by lowering the VLDL secretion," *European Journal of Pharmacology*, vol. 431, no. 1, pp. 127–131, 2001.

[55] A. J. van Boven, J. W. Jukema, A. H. Zwinderman, H. J .G. M. Crijns, K. I. Lie, and A. V. G. Bruschke, "Reduction of transient myocardial ischemia with pravastatin in addition to the conventional treatment in patients with angina pectoris," *Circulation*, vol. 94, no. 7, pp. 1503–1505, 1996.

[56] M. Shiomi, S. Yamada, Y. Amano, T. Nishimoto, and T. Ito, "Lapaquistat acetate, a squalene synthase inhibitor, changes macrophage/lipid-rich coronary plaques of hypercholesterolaemic rabbits into fibrous lesions," *British Journal of Pharmacology*, vol. 154, no. 5, pp. 949–957, 2008.

[57] A. Mortensen, B. F. Hansen, J. F. Hansen et al., "Comparison of the effects of fish oil and olive oil on blood lipids and aortic atherosclerosis in Watanabe heritable hyperlipidaemic rabbits," *British Journal of Nutrition*, vol. 80, no. 6, pp. 565–573, 1998.

[58] A. H. Lichtenstein and A. V. Chobanian, "Effect of fish oil on atherogenesis in Watanabe heritable hyperlipidemic rats," *Arteriosclerosis*, vol. 10, no. 4, pp. 597–606, 1990.

[59] S. L. Pfister, M. Rosolowsky, J. M. Schmitz, F. J. Clubb, and W. B. Campbell, "Eicosapentaenoic acid alters vascular reactivity and platelet adhesion in Watanabe heritable hyperlipidemic rabbits," *European Journal of Pharmacology*, vol. 161, no. 1, pp. 85–89, 1989.

[60] S. Rich, J. F. Miller, S. Charous et al., "Development of atherosclerosis in genetically hyperlipidemic rabbits during chronic fish-oil ingestion," *Arteriosclerosis*, vol. 9, no. 2, pp. 189–194, 1989.

[61] F. J. Clubb, J. M. Schmitz, M. M. Butler, L. M. Buja, J. T. Willerson, and W. B. Campbell, "Effect of dietary omega-3 fatty acid on serum lipids, platelet function, and atherosclerosis in Watanabe Heritable Hyperlipidemic rabbits," *Arteriosclerosis*, vol. 9, no. 4, pp. 529–537, 1989.

[62] T. Kita, Y. Nagano, M. Yokode et al., "Probucol prevents the progression of atherosclerosis in Watanabe heritable hyperlipidemic rabbit, an animal model for familial hypercholesterolemia," *Proceedings of the National Academy of Sciences of the United States of America*, vol. 84, no. 16, pp. 5928–5931, 1987.

[63] T. E. Carew, D. C. Schwenke, and D. Steinberg, "Antiatherogenic effect of probucol unrelated to its hypocholesterolemic effect: evidence that antioxidants in vivo can selectively inhibit low density lipoprotein degradation in macrophage-rich fatty streaks and slow the progression of atherosclerosis in the Watanabe heritable hyperlipidemic rabbit," *Proceedings of the National Academy of Sciences of the United States of America*, vol. 84, no. 21, pp. 7725–7729, 1987.

[64] F. de Nigris, T. Youssef, S. Ciafré et al., "Evidence for oxidative activation of c-Myc-dependent nuclear signaling in human coronary smooth muscle cells and in early lesions of Watanabe heritable hyperlipidemic rabbits: protective effects of vitamin E," *Circulation*, vol. 102, no. 17, pp. 2111–2117, 2000.

[65] N. Yoshida, H. Murase, T. Kunieda et al., "Inhibitory effect of a novel water-soluble vitamin E derivative on atherosclerosis in rabbits," *Atherosclerosis*, vol. 162, no. 1, pp. 111–117, 2002.

[66] N. Yamada, S. Ishibashi, H. Shimano et al., "Role of monocyte colony-stimulating factor in foam cell generation," *Proceedings of the Society for Experimental Biology and Medicine*, vol. 200, no. 2, pp. 240–244, 1992.

[67] J. Shindo, T. Ishibashi, K. Yokoyama et al., "Granulocyte-macrophage colony-stimulating factor prevents the progression of atherosclerosis via changes in the cellular and extracellular composition of atherosclerotic lesions in Watanabe heritable hyperlipidemic rabbits," *Circulation*, vol. 99, no. 16, pp. 2150–2156, 1999.

[68] A. V. Chobanian, C. C. Haudenschild, C. Nickerson, and S. Hope, "Trandolapril inhibits atherosclerosis in the Watanabe heritable hyperlipidemic rabbit," *Hypertension*, vol. 20, no. 4, pp. 473–477, 1992.

[69] S. Hope, P. Brecher, and A. V. Chobanian, "Comparison of the effects of AT receptor blockade and angiotensin converting enzyme inhibition on atherosclerosis," *American Journal of Hypertension*, vol. 12, no. 1 I, pp. 28–34, 1999.

[70] H. Koike, "New pharmacologic aspects of CS-866, the newest angiotensin II receptor antagonist," *American Journal of Cardiology*, vol. 87, no. 8, supplement 1, pp. 33c–36c, 2001.

[71] T. Imanishi, A. Kuroi, H. Ikejima et al., "Effects of angiotensin converting enzyme inhibitor and angiotensin II receptor antagonist combination on nitric oxide bioavailability and atherosclerotic change in Watanabe heritable hyperlipidemic rabbits," *Hypertension Research*, vol. 31, no. 3, pp. 575–584, 2008.

[72] T. Imanishi, H. Tsujioka, H. Ikejima et al., "Renin inhibitor aliskiren improves impaired nitric oxide bioavailability and protects against atherosclerotic changes," *Hypertension*, vol. 52, no. 3, pp. 563–572, 2008.

[73] J. L. M. van Niekerk, Th. Hendriks, H. H. M. de Boer, and A. Van 't Laar, "Does nifedipine suppress atherogenesis in WHHL rabbits?" *Atherosclerosis*, vol. 53, no. 1, pp. 91–98, 1984.

[74] A. V. Chobanian, "The effects of ACE inhibitors and other antihypertensive drugs on cardiovascular risk factors and

atherogenesis," *Clinical Cardiology*, vol. 13, no. 6, pp. VII43–VII48, 1990.

[75] H. Hosomi, S. Katsuda, and Y. Watanabe, "Effect of atherosclerosis on the responsiveness of the rapidly acting arterial pressure control system in WHHL rabbits," *Cardiovascular Research*, vol. 20, no. 3, pp. 195–200, 1986.

[76] M. Sata and D. Fukuda, "Crucial role of renin-angiotensin system in the pathogenesis of atherosclerosis," *Journal of Medical Investigation*, vol. 57, no. 1-2, pp. 12–25, 2010.

[77] M. Ogawa, S. Ishino, T. Mukai et al., "F-FDG accumulation in atherosclerotic plaques: immunohistochemical and PET imaging study," *Journal of Nuclear Medicine*, vol. 45, no. 7, pp. 1245–1250, 2004.

[78] J. Meding, M. Urich, K. Licha et al., "Magnetic resonance imaging of atherosclerosis by targeting extracellular matrix deposition with Gadofluorine M," *Contrast Media & Molecular Imaging*, vol. 2, no. 3, pp. 120–129, 2007.

[79] H. Steen, J. A. C. Lima, S. Chatterjee et al., "High-resolution three-dimensional aortic magnetic resonance angiography and quantitative vessel wall characterization of different atherosclerotic stages in a rabbit model," *Investigative Radiology*, vol. 42, no. 9, pp. 614–621, 2007.

[80] A. Iwata, S. I. Miura, S. Imaizumi, B. Zhang, and K. Saku, "Measurement of atherosclerotic plaque volume in hyperlipidemic rabbit aorta by intravascular ultrasound," *Journal of Cardiology*, vol. 50, no. 4, pp. 229–234, 2007.

[81] M. Ogawa, Y. Magata, T. Kato et al., "Application of F-FDG PET for monitoring the therapeutic effect of antiinflammatory drugs on stabilization of vulnerable atherosclerotic plaques," *Journal of Nuclear Medicine*, vol. 47, no. 11, pp. 1845–1850, 2006.

Research Article

Journal of Labelled Compounds and Radiopharmaceuticals

Received 5 September 2011, Revised 7 November 2011, Accepted 13 November 2011 Published online 12 December 2011 in Wiley Online Library

(wileyonlinelibrary.com) DOI: 10.1002/jlcr.1954

A novel bifunctional chelating agent based on *bis*(hydroxamamide) for ^{99m}Tc labeling of polypeptides

Masahiro Ono,[a,b]* Masatsugu Ohgami,[a] Mamoru Haratake,[a] Hideo Saji,[b] and Morio Nakayama[a]**

This paper describes the synthesis and biological evaluation of a novel bifunctional chelating agent (BCA) based on *bis*(hydroxamamide) for ^{99m}Tc labeling of polypeptides. We successfully designed and synthesized $C_3(BHam)_2$-COOH as a new BCA. $C_3(BHam)_2$-COOH formed a stable ^{99m}Tc complex and enabled us to prepare ^{99m}Tc-labeled polypeptides by using a 2,3,5,6-tetrafluorophenol (TFP) active ester of $C_3(BHam)_2$-COOH. ^{99m}Tc-$C_3(BHam)_2$-HSA prepared with $C_3(BHam)_2$-TFP was stable in both murine plasma and an excess of L-cysteine without any dissociation of ^{99m}Tc from polypeptides. Furthermore, the blood clearance of ^{99m}Tc-$C_3(BHam)_2$-HSA in mice was similar to that of ^{125}I-HSA, suggesting that $C_3(BHam)_2$-COOH retained stable binding between ^{99m}Tc and the polypeptides *in vivo*. When ^{99m}Tc-$C_3(BHam)_2$-NGA was injected into mice, the radioactivity showed high hepatic uptake early on and a rapid clearance from the liver, indicating that $C_3(BHam)_2$-COOH did not affect the pharmacokinetics of polypeptides *in vivo* and gave radiometabolites, which displayed a rapid elimination from the liver. Such characteristics would render $C_3(BHam)_2$-COOH attractive as a new BCA for ^{99m}Tc labeling of polypeptides.

Keywords: ^{99m}Tc; bifunctional chelating agent; polypeptide; hydroxamamide

Introduction

Many polypeptides such as antibodies, single-chain Fv fragments, diabodies, affibodies, minibodies, and bioactive peptides have been used as scaffolds of radiolabeled probes for targeted imaging of sites of tumors, infection, and thrombosis.[1–10] Among radionuclides for radiolabeling of these polypeptides, ^{99m}Tc is ideal for scintigraphic imaging because of its excellent physical properties, low cost, and ready availability.[11,12] Generally, polypeptides do not possess binding sites to form ^{99m}Tc chelates of high stability *in vivo*. To prepare ^{99m}Tc-labeled peptides for application *in vivo*, therefore, one must incorporate appropriate chelating agents into polypeptide molecules.

^{99m}Tc labeling using bifunctional chelating agents (BCAs), which possess both a binding site for polypeptides and a site for complexation with ^{99m}Tc, is required. It has been reported that tetradentate ligands with N_3S or N_2S_2 (containing one or two thiol groups)[13–15] and hydrazino nicotinamide (HYNIC) (thiol-free chelating agent)[16–19] serve as a BCA for ^{99m}Tc labeling. However, some N_3S or N_2S_2 ligands require harsh ^{99m}Tc complexation (elevated temperatures or high pH) to prepare ^{99m}Tc chelates with high radiochemical yields.[13–15] When ^{99m}Tc-HYNIC-labeled polypeptides were administered *in vivo*, they showed not only localized radioactivity in target tissues but also strong, persistent radioactivity in non-target tissues.[17]

To improve BCAs, we have developed 4′-aminomethyl-*N*,*N*′-trimethylene bisbenzohydroxamamide [$C_3(BHam)_2$-NH_2], which has $C_3(BHam)_2$ for chelating with ^{99m}Tc and a primary amino group for binding with polypeptides (Figure 1).[20–24] A recent report showed that the ^{99m}Tc complexes of benzohydroxamamide (BHam) possessed square base pyramid coordination geometry, and the equatorial plane was formed by two-amine nitrogen and two-oxime oxygen atoms in a trans-orientation, whereas the oxo core of the Tc(V) occupied the apical position.[25] Indeed, $C_3(BHam)_2$-NH_2 provided stable ^{99m}Tc-labeled antibodies in mild conditions to image tumor sites in tumor-bearing mice.[23] However, as $C_3(BHam)_2$-NH_2 cannot directly conjugate to polypeptides, *N*-(6-maleimidocaproyloxy)succinimide (EMCS) and 2-iminothiolane (2-IT) were essential for the preparation of ^{99m}Tc-labeled polypeptides by using $C_3(BHam)_2$-NH_2 as a BCA. When $C_3(BHam)_2$-NH_2 is applied to ^{99m}Tc labeling for lower molecular weight polypeptides, the incorporation of spacers (EMCS and 2-IT) between ^{99m}Tc-$C_3(BHam)_2$ and polypeptides may affect the pharmacokinetics and bioactivity of the polypeptides.[26,27]

[a]*Graduate School of Biomedical Sciences, Nagasaki University, 1-14 Bunkyo-machi, Nagasaki 852-8521, Japan*

[b]*Graduate School of Pharmaceutical Sciences, Kyoto University, 46-29 Yoshida Shimoadachi-cho, Sakyo-ku, Kyoto 606-8501, Japan*

**Correspondence to: Masahiro Ono, Graduate School of Pharmaceutical Sciences, Kyoto University, 46-29 Yoshida Shimoadachi-cho, Sakyo-ku, Kyoto 606-8501, Japan.*
E-mail: ono@pharm.kyoto-u.ac.jp

***Correspondence to: Morio Nakayama, Graduate School of Biomedical Sciences, Nagasaki University, 1-14 Bunkyo-machi, Nagasaki 852-8521, Japan.*
E-mail: morio@nagasaki-u.ac.jp

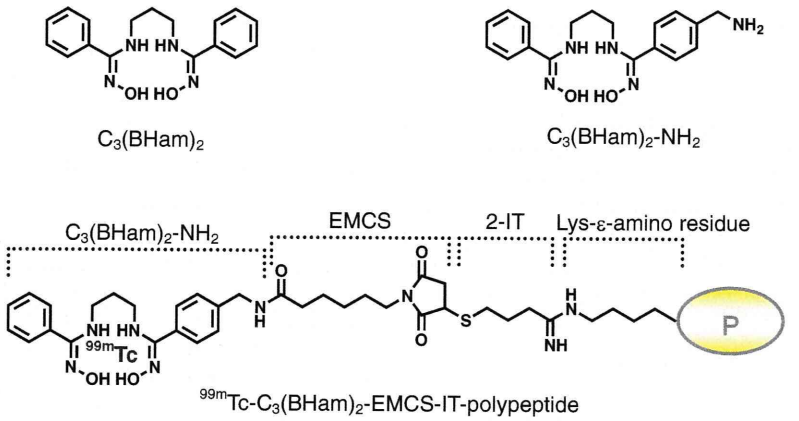

Figure 1. Chemical structure of $C_3(BHam)_2$, $C_3(BHam)_2$-NH_2, and ^{99m}Tc-$C_3(BHam)_2$-EMCS-IT-polypeptide.

The objective of this study was to develop a novel BCA based on $C_3(BHam)_2$, which can be introduced into polypeptides without a long linker such as EMCS and 2-IT. We designed and synthesized 4′-carboxyl-*N*,*N*′-trimethylene bisbenzohydroxamamide [$C_3(BHam)_2$-COOH], which has carboxylic acid for binding with the lys-ε-amino group of polypeptides. Next, using $C_3(BHam)_2$-COOH, we investigated the labeling of ^{99m}Tc with human serum albumin (HSA) as a model polypeptide and evaluated the stability of ^{99m}Tc-$C_3(BHam)_2$-HSA *in vitro* and *in vivo*. Furthermore, we used galactosyl-neoglycoalbumin (NGA) as a model polypeptide and evaluated the pharmacokinetics of radiometabolites formed in the liver after the injection of ^{99m}Tc-$C_3(BHam)_2$-NGA into mice.

Materials and methods

Reagents and chemicals

Proton nuclear magnetic resonance (^{1}H NMR) spectra were recorded on a Varian Gemini 300 (300 MHz) (Varian Medical Systems, Inc., Calfornia, USA). Electron impact mass spectra (EI-MS) and fast atom bombardment mass spectra (FAB-MS) were obtained with a JEOL IMS-DX300 mass spectrometer (JEOL Ltd., Tokyo, Japan). Na[^{125}I]I (3.7 GBq/mL, 0.01 N NaOH solution) was obtained from MP Biomedicals. [^{99m}Tc]Pertechnetate ($^{99m}TcO_4^-$) (111 MBq/mL) was purchased from Nihon-Medi-Physics (Tokyo, Japan). Size-exclusion HPLC (SE-HPLC) was performed using a TSK G3000SW (7.8 × 300 mm) column (Tosoh Corporation, Tokyo, Japan), eluted with 0.1 M phosphate buffer (PB) (pH 7.0) containing 0.3 M sodium chloride at a flow rate of 0.5 mL/min. Reversed-phase HPLC (RP-HPLC) was performed with a Cosmosil 5 C_{18}-MS column (4.6 × 150 mm, Nacalai Tesque, Kyoto, Japan) at a flow rate of 1 mL/min with a gradient mobile phase from 85% A (PB, 0.01 M, pH 7.4) and 15% B (acetonitrile) to 20% A and 80% B in 10 min. Cellulose acetate electrophoresis (CAE) was run on Separax SP (Joko, Tokyo, Japan) at a constant current of 0.8 mA/cm for 30 min in 0.072 M veronal buffer (pH 8.6). The distance migrated by HSA was determined by Ponceau 3R staining.

Synthesis of benzohydroxamamide

To a solution of hydroxylammonium chloride (10.5 g, 145.2 mmol) and $NaHCO_3$ (12.3 g, 146.0 mmol) in H_2O (40 mL) was gradually added a solution of benzonitrile (15.3 g, 145.2 mmol) in EtOH (100 mL), and the reaction mixture was stirred at 80 °C for 4 h. EtOH was removed *in vacuo*, and the mixture was extracted with ethyl acetate. After drying of the organic layer on Na_2SO_4, evaporation gave 16.6 g of BHam (83.1%). ^{1}H NMR (DMSO-d_6) δ: 5.81 (s, 2H, -NH_2), 7.36–7.38 (m, 3H, aromatic), 7.66–7.69 (m, 2H, aromatic), 9.64 (s, 1H, -NOH).

Synthesis of O-carbethoxybenzohydroxamamide (**1**)

To a solution of BHam (19.0 g, 140.0 mmol) in dry acetone (90 mL) was gradually added a solution of ethyl chlorocarbonate (16.8 g, 156.0 mmol) in acetone (30 mL) in an ice bath for 1 h. After a 5% NaOH solution (126 mL) was added, the mixture was stirred at room temperature for 1 h. The precipitate formed was filtered, and the residue was recrystallized from H_2O–acetone (4:3) to give 15.9 g of **1** (54.9%). ^{1}H NMR ($CDCl_3$) δ: 1.37 (t, 3H, –CH_3), 4.33 (q, 2H, J = 7.2 Hz, –CH_2), 5.11 (s, broad, 2H, -NH_2), 7.41–7.48 (m, 3H, aromatic), 7.68–7.71 (m, 2H, aromatic).

Synthesis of 3-phenyl-Δ^2-1,2,4-oxadiazolin-5-one (***2***)

To a solution of **1** (15.8 g, 75.7 mmol) in 5% NaOH solution (80 mL) was added excess acetic acid (26.3 mL, 460 mmol). The precipitate formed was filtered to give 10.7 g of **2** (87.5%). ^{1}H NMR (DMSO-d_6) δ: 7.56-7.67 (m, 3H, aromatic), 7.81–7.85 (q, 2H, J = 6.3 Hz, aromatic).

Synthesis of potassium 3-phenyl-Δ^2-1,2,4-oxadiazolin-5-one (***3***)

To a solution of **2** (7.50 g, 46.3 mmol) in MeOH (20 mL) was added a solution of KOH (2.60 g, 46.3 mmol) in MeOH (30 mL). After the mixture was stirred at room temperature for 1 h, evaporation gave 8.97 g of **3** (96.8%). ^{1}H NMR (DMSO-d_6) δ: 7.37–7.42 (m, 3H, aromatic), 7.76–7.80 (m, 2H, aromatic).

Synthesis of 3-phenyl-4-(3-bromopropyl)-Δ^2-1,2,4-oxadiazolin-5-one (***4***)

To a solution of **3** (9.28 g, 32.8 mmol) in DMF (31 mL) was added 1,3-dibromopropane (19.9 g, 98.4 mmol) in DMF (25 mL). The reaction mixture was stirred at room temperature for 3 days. After the filtrating precipitate of potassium bromide was filtered and the solvent was removed, the residue was purified by silica gel chromatography (ethyl acetate/hexane = 1:5) to give 4.56 g of **4** (49.1%). ^{1}H NMR ($CDCl_3$) δ: 2.22–2.26 (m, 2H, -$NCH_2\underline{CH_2}CH_2Br$), 3.35 (t, 2H, -$\underline{NCH_2}CH_2CH_2Br$), 3.86 (t, 2H, -$NCH_2CH_2\underline{CH_2}Br$), 7.58–7.63 (m, 5H, aromatic).

*Synthesis of 4-carboxylbenzohydroxamamide methyl ester (BHam-COOMe, **5**)*

The reaction mixture of 4-cyanobenzoic acid methyl ester (10.0 g, 61.8 mmol), $NaHCO_3$ (5.35 g, 66.7 mmol), and hydroxylammonium chloride (4.30 g, 61.8 mmol) in MeOH (120 mL) was stirred at room temperature for 30 min. The mixture was then stirred at 80–90 °C for 3 h. After it had cooled to room temperature, 200 mL of water was added to produce a precipitate. **5** was obtained after washing the precipitate with ether in a yield of 68.6% (8.24 g). ^{1}H NMR ($CDCl_3$) δ: 3.94 (s, 3H, $-CH_3$), 4.89 (s, broad, 2H, $-NH_2$), 7.72 (t, 2H, aromatic), 8.89 (t, 2H, aromatic).

*Synthesis of 3-(4-carboxylphenyl)-Δ^2-1,2,4-oxadiazolin-5-one methyl ester (**6**)*

To a suspension of **5** (4.96 g, 25.5 mmol) in 1,4-dioxane (35 mL) was added 1'-carbonyldiimidazole (5.30 g, 30.6 mmol). The mixture was stirred at 110 °C for 30 min. The solvent was removed, the residue was dissolved in water, and 3 N HCl was added to produce a precipitate. The precipitate was washed with water, ether, and ethyl acetate to give 4.91 g of **6** (87.5%). ^{1}H NMR (DMSO-d_6) δ: 3.90 (s, 3H, $-CH_3$), 7.96 (d, 2H, J = 8.7 Hz, aromatic), 8.15 (t, 2H, aromatic).

*Synthesis of potassium 3-(4-carboxylphenyl)-Δ^2-1,2,4-oxadiazolin-5-one methyl ester (**7**)*

To a solution of **6** (8.62 g, 39.2 mmol) in MeOH (23 mL) was added a solution of KOH (2.25 g, 40.0 mmol) in MeOH (28 mL). After the reaction mixture was stirred at room temperature for 1 h, evaporation of the solvent gave 9.78 g of **7** (96.6%). ^{1}H NMR (DMSO-d_6) δ: 3.87 (s, 3H, $-CH_3$), 7.93 (t, 2H, aromatic), 8.00 (t, 2H, aromatic).

*Synthesis of methyl 4-(4,5-dihydro-5-oxo-4-(3-(5-oxo-3-phenyl-1,2,4-oxadiazol-4-yl)propyl)-1,2,4-oxadiazol-3-yl)benzoate (**8**)*

To a solution of **4** (1.15 g, 4.06 mmol) in DMF (20 mL) was added a solution of **7** (1.11 g, 4.30 mmol) in DMF (20 mL) at room temperature. The reaction mixture was then stirred at 40 °C for 7 days. The solvent was evaporated, water was added, and the mixture was extracted with ethyl acetate. The organic layer was dried over Na_2SO_4 and filtered. The residue was purified by silica gel chromatography (ethyl acetate/hexane = 1:2) to give 850 mg of **8** (49.6%). ^{1}H NMR (DMSO-d_6) δ: 1.77 (m, 2H, $-CH_2\underline{CH_2}CH_2-$), 3.55–3.62 (q, 4H, J = 7.2 Hz, $-\underline{CH_2}CH_2\underline{CH_2}-$), 3.93 (s, 3H, $-CH_3$), 7.56–7.60 (m, 4H, aromatic), 7.64–7.69 (m, 1H, aromatic), 7.75 (d, 2H, J = 7.8 Hz, aromatic), 8.12 (d, 2H, J = 8.1 Hz, aromatic). EI-MS calc $C_{21}H_{18}N_4O_6$ (M^+): m/z 422, found: 422.

Synthesis of C_3(BHam)$_2$-COOH

8 (850 mg, 2.01 mmol) was added to 5 mL of 1 N NaOH, and the mixture was heated with stirring at 90–100 °C for 1.5 h, then allowed to cool to room temperature. The pH was adjusted to 3 with 1 N HCl. The mixture was neutralized with 1 N NaOH, and the solvent was removed *in vacuo*. The residue was purified by silica gel chromatography (MeOH/$CHCl_3$/acetic acid = 10:50:1) to give 620 mg of C_3(BHam)$_2$-COOH (61.5%). ^{1}H NMR (DMSO-d_6) δ: 1.57 (m, 2H, $-CH_2\underline{CH_2}CH_2-$), 3.00–3.08 (m, 4H, $-\underline{CH_2}CH_2\underline{CH_2}-$), 7.53–7.62 (m, 7H, aromatic), 8.05 (d, 2H, J = 9.0 Hz, aromatic), 8.92 (s, 1H, -COOH). FAB-MS calc $C_{18}H_{21}N_4O_4$ (MH^+): m/z 357, found: 357.

Preparation of ^{99m}Tc-C_3(BHam)$_2$-COOH

A solution of C_3(BHam)$_2$-COOH in DMSO (0.1 M) was prepared. This solution (5 μL) was added to H_2O (495 μL). A solution of stannous tartrate (375 μL, 3×10^{-4} M) in H_2O and $Na^{99m}TcO_4$ (74 MBq/mL, 125 μL) was then added. After incubation for 15 min, radiochemical yields of ^{99m}Tc-C_3(BHam)$_2$-COOH were determined by RP-HPLC, CAEP, and TLC.

Preparation of ^{99m}Tc-C_3(BHam)$_2$-TFP

2,3,5,6-Tetrafluorophenol (TFP) (2 mg) was added to a solution of ^{99m}Tc-C_3(BHam)$_2$-COOH in saline (200 μL). Next, 1-ethyl-3-(3-dimethylaminopropyl)carbodiimide hydrochloride (EDC) (4 mg) was added, the reaction mixture was stirred at room temperature for 30 min, DMSO (60 μL) was added, and the mixture was purified using Sep-Pak. The Sep-Pak was replaced with water. The reaction mixture (260 μL) was applied, the column was washed with water (6 mL) and diethylether (1 mL), and ^{99m}Tc-C_3(BHam)$_2$-TFP was eluted with acetonitrile (1 mL). After evaporation of the acetonitrile, the radioactivity in the residue was analyzed by SE-HPLC and CAEP.

Preparation of ^{99m}Tc-C_3(BHam)$_2$-HSA

To 200 μL of HSA solution (10 mg/mL in 0.1 M carbonate buffer, pH 9.5) was added an equal volume of ^{99m}Tc-C_3(BHam)$_2$-TFP prepared above, and the reaction mixture was incubated for 1 h at room temperature. ^{99m}Tc-C_3(BHam)$_2$-HSA was then purified by the centrifuged column procedure using a Sephadex G-50 column equilibrated and eluted with PB (0.1 M, pH 7.4). The radiochemical yield was assessed by SE-HPLC and CAEP.

Preparation of ^{99m}Tc-C_3(BHam)$_2$-NGA

Galactosyl-neoglycoalbumin was synthesized by conjugation of cyanomethyl-2,3,4,6-tetra-*O*-acetyl-1-thio-β-*D*-galactopyranoside, synthesized according to the procedure of Lee *et al.*,[28] with HSA. The phenol–sulfuric acid reaction indicated that 25 galactose units were attached to each HSA molecule.[29] ^{99m}Tc-C_3(BHam)$_2$-NGA was prepared similar to ^{99m}Tc-C_3(BHam)$_2$-HSA, and radiochemical yield was assessed by SE-HPLC and CAEP.

Preparation of ^{125}I-HSA

To 200 μL of HSA solution (4 mg/mL in 0.1 M PB, pH 7.4) was added 1 μL of $Na^{125}I$ (3.7 GBq/mL) solution and 10 μL of chloramine-T solution (2 mg/mL in 0.1 M PB, pH 7.4). The reaction mixture was incubated for 10 min. A solution of $NaHSO_3$ (1 mg/mL, 6 μL) was added, and the mixture was purified by the centrifuged column procedure using a Sephadex G-50 column equilibrated and eluted with PB (0.1 M, pH 7.4). The radiochemical yield of ^{125}I-HSA was assessed by CAEP and TLC.

Stability of ^{99m}Tc-C_3(BHam)$_2$-HSA *in vitro*

^{99m}Tc-C_3(BHam)$_2$-HSA (50 μL, 8.3 kBq) was diluted 20-fold with 0.1 M PB (pH 7.4, 200 μL) or freshly prepared murine plasma, and the solution was incubated at 37 °C. After 1, 3, 6, and 24 h of incubation, the radioactivity of ^{99m}Tc-C_3(BHam)$_2$-HSA was analyzed by CAEP. To a solution of ^{99m}Tc-C_3(BHam)$_2$-HSA (12.2 kBq) in 0.1 M PB (pH 7.4, 135 μL) was added L-cysteine (15 μL, 5×10^{-6} to 5×10^{-2} M). After incubation for 1 h at 37 °C, the radioactivity of the reaction mixture was analyzed by SE-HPLC. ^{99m}Tc-cysteine was prepared by incubating for 1 h at room temperature after mixing a solution of 0.1 M L-cysteine (100 μL) with an aqueous solution of stannous tartrate (75 μL, 3×10^{-4} M) and $Na^{99m}TcO_4$ (25 μL, 3.7 MBq).

Experiments in vivo

Animal experiments were conducted in accordance with our institutional guidelines and approved by the Nagasaki University Animal Care Committee. Biodistribution experiments were performed by intravenously administering ^{99m}Tc-C_3(BHam)$_2$-HSA (37 MBq/mL in 66 mM PB, pH 7.4) or ^{125}I-HSA (37 kBq/mL in 66 mM PB, pH 7.4) to 5-week-old male ddY mice (20–25 g). Groups of four to five mice each were administered 100 μL (3.7 kBq) of ^{99m}Tc-C_3(BHam)$_2$-HSA prior to sacrifice at 5, 10, 30, and 60 min postinjection by decapitation. Tissues of interest were removed and weighed, and radioactivity was measured with an auto well gamma counter. Data in the biodistribution experiments were analyzed using the unpaired *t*-test. Differences were considered statistically significant when the *p* value was less than 0.05.

The concentration of ^{99m}Tc-C_3(BHam)$_2$-NGA was adjusted to 90 μg/mL with PB (66 mM, pH 7.4). Biodistribution experiments were performed by intravenously administering ^{99m}Tc-C_3(BHam)$_2$-NGA to 6-week-old male ddY mice (25–30 g). Groups of five to eight mice each were administered 9 μg of ^{99m}Tc-C_3(BHam)$_2$-NGA prior to sacrifice at 5, 10, 30, 60, 180, and 360 min postinjection by decapitation. Tissues of interest were removed and weighed, and radioactivity was measured with an auto well gamma counter.

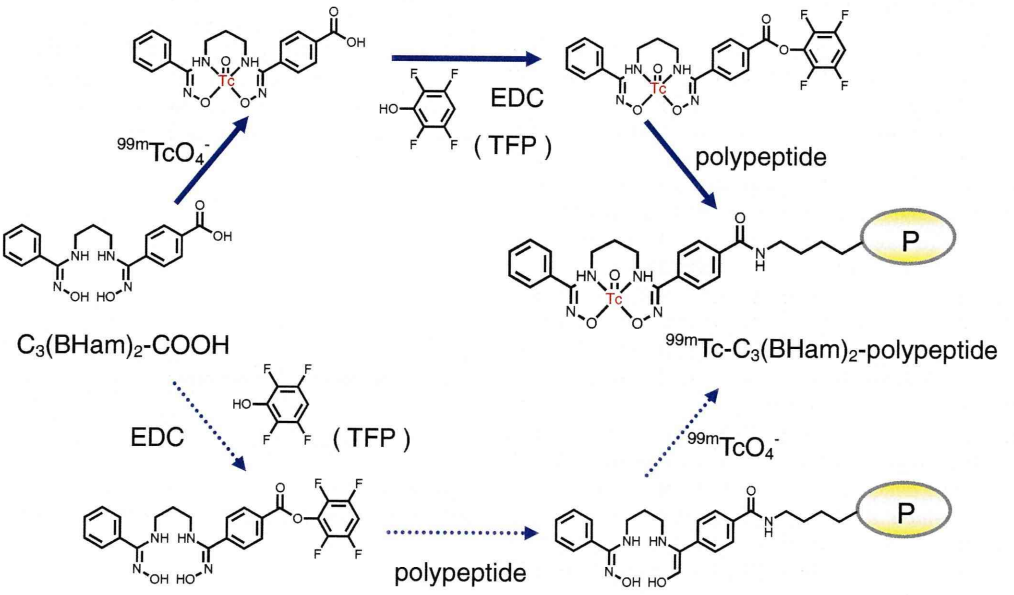

Figure 2. Two schemes for ^{99m}Tc labeling of polypeptides using C_3(BHam)$_2$-COOH.

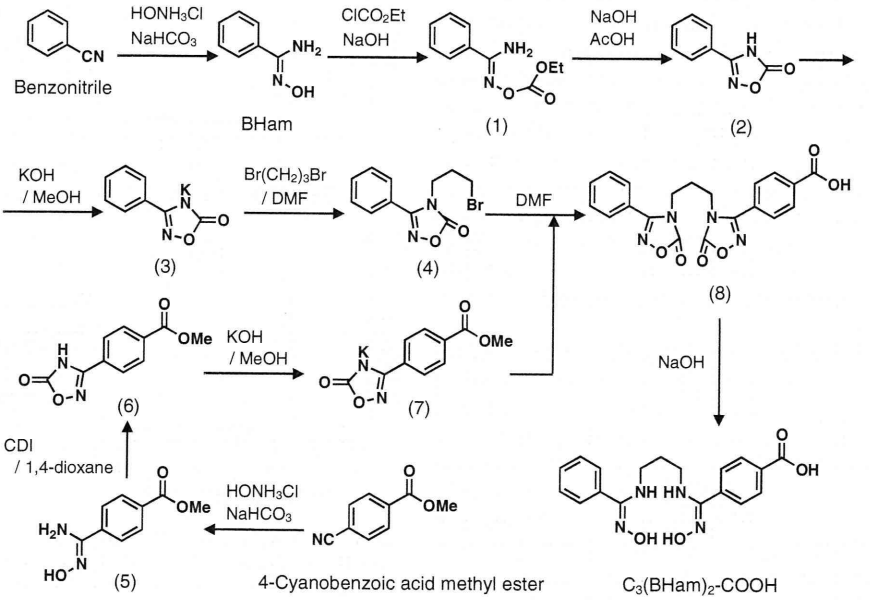

Scheme 1. Synthesis of C_3(BHam)$_2$-COOH.

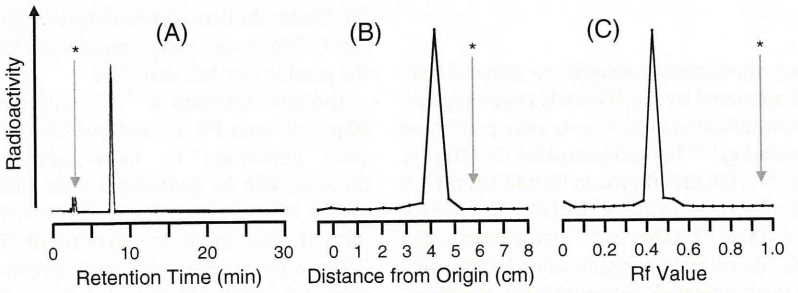

Figure 3. Radiochromatograms of ^{99m}Tc-C_3(BHam)$_2$-COOH obtained by RP-HPLC (A), CAEP (B), and TLC (C). Arrows with single asterisks show $^{99m}TcO_4^-$.

Results and discussion

In the present study, in order to introduce ^{99m}Tc-C_3(BHam)$_2$ into polypeptides, we designed and synthesized C_3(BHam)$_2$ which has a carboxylic acid for binding to the lys-ε-amino group of polypeptides. As shown in Figure 1, we tried two methods of preparing ^{99m}Tc-labeled polypeptides by using C_3(BHam)$_2$-COOH as a BCA. Considering the half-life of ^{99m}Tc, and convenience of labeling experiments or radiation exposure, a method of labeling polypeptides with ^{99m}Tc after conjugation with a BCA is preferred. Therefore, first of all, we tried to synthesize a TFP active ester of C_3(BHam)$_2$-COOH in order to conjugate polypeptides with a BCA before ^{99m}Tc labeling (Figure 2, the scheme shown with a dotted line). We performed the reaction of (BHam)$_2$-COOH with TFP under several different conditions. However, all the reactions gave multiple products, and we could not obtain C_3(BHam)$_2$-TFP. This may be one of the reasons why C_3(BHam)$_2$-TFP reacts with an active secondary amino group or hydroxy group in the hydroxamamide scaffold. As we had difficulty producing C_3(BHam)$_2$-TFP, we used an alternative method to prepare ^{99m}Tc-labeled polypeptides, through the conjugation of polypeptides with ^{99m}Tc-C_3(BHam)$_2$-TFP after active esterification of ^{99m}Tc-C_3(BHam)$_2$-COOH prepared by labeling C_3(BHam)$_2$-COOH with ^{99m}Tc (Figure 2). Previous papers have reported that ^{99m}Tc-labeled polypeptides were successfully prepared using N_2S_2 and N_3S type ligands as BCAs by such a pre-chelating method without a loss of bioactivity.[13,14,30] Furthermore, as the chemical form of ^{99m}Tc-labeled polypeptides is the same even using different methods, in the present study, we synthesized ^{99m}Tc-labeled polypeptides through the latter approach, and evaluated the utility of C_3(BHam)$_2$-COOH as a BCA for ^{99m}Tc labeling.

C_3(BHam)$_2$-COOH was synthesized by using benzonitrile and 4-cyanobenzoic acid methyl ester as the starting materials according to the route shown in Scheme 1. Compounds **4** and **6** were synthesized as reported previously. **6** was converted to its potassium salt (**7**). **7** was reacted with **4** to give **8**. **8** was hydrolyzed in a 5% NaOH solution to give C_3(BHam)$_2$-COOH in a total yield of 5.7%.

The radioactivity of the reaction mixture of C_3(BHam)$_2$-COOH and ^{99m}Tc was analyzed by RP-HPLC. The radioactivity of $^{99m}TcO_4^-$ at 3 min disappeared, and a new peak derived from ^{99m}Tc-C_3(BHam)$_2$-COOH was detected at a retention time of 7 min (Figure 3(A)). A new peak was detected 4 cm (anode) from the origin in the analysis by CAEP (Figure 3(B)) and at Rf = 0.4 in the analysis by TLC (Figure 3(C)). The results suggested that ^{99m}Tc-C_3(BHam)$_2$-COOH was produced, because radioactivity of $^{99m}TcO_4^-$ was detected at 6 cm (anode) by CAEP and at Rf = 1.0 by TLC. The radiochemical yield of ^{99m}Tc-C_3(BHam)$_2$-COOH was over 93% in the RP-HPLC, TLC, and CAEP analyses. These results indicated that C_3(BHam)$_2$-COOH can function as the coordinating site of ^{99m}Tc in mild labeling conditions.

After the active esterification of ^{99m}Tc-C_3(BHam)$_2$-COOH with TFP using EDC, we analyzed the radioactivity eluted from the Sep-Pak column by RP-HPLC. The peak for ^{99m}Tc-C_3(BHam)$_2$-TFP was observed at a retention time of 14 min, which was later than that

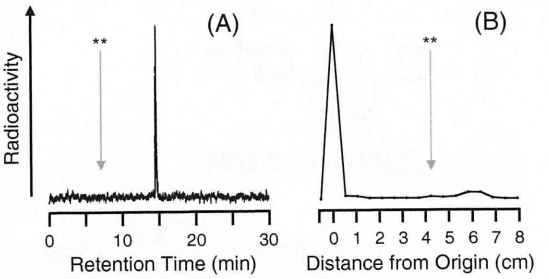

Figure 4. Radiochromatograms of ^{99m}Tc-C_3(BHam)$_2$-TFP obtained by RP-HPLC (A) and CAEP (B). Arrows with double asterisks show ^{99m}Tc-C_3(BHam)$_2$-COOH.

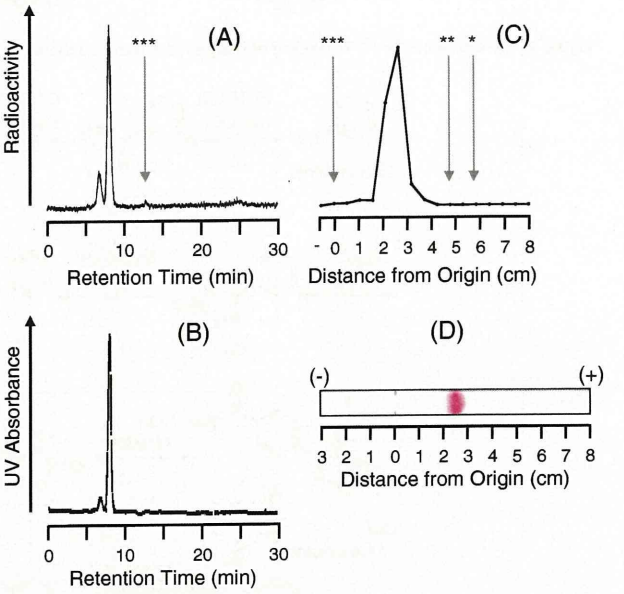

Figure 5. SE-HPLC profiles of ^{99m}Tc-C_3(BHam)$_2$-HSA (radioactivity, A) and unmodified HSA (UV absorbance 254 nm, B). A typical radioactivity profile of ^{99m}Tc-C_3(BHam)$_2$-HSA (C) and Ponceau 3R staining of unmodified HSA analyzed by CAEP (D). Arrows with single, double, and triple asterisks show $^{99m}TcO_4^-$, ^{99m}Tc-C_3(BHam)$_2$-COOH, and ^{99m}Tc-C_3(BHam)$_2$-TFP, respectively.

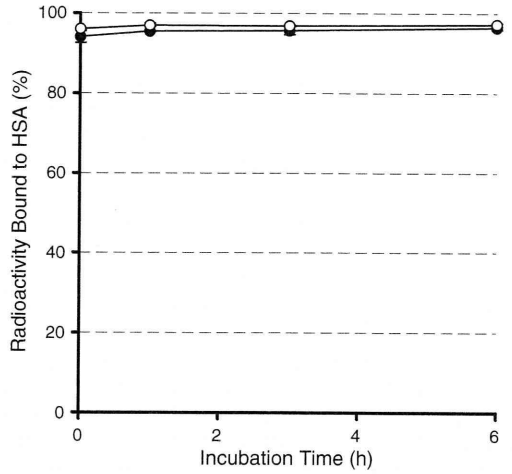

Figure 6. Percent radioactivity in HSA fractions following incubation of ^{99m}Tc-C_3(BHam)$_2$-HSA in phosphate buffer (●) and murine plasma (○) at 37 °C. Each value was determined by CAEP.

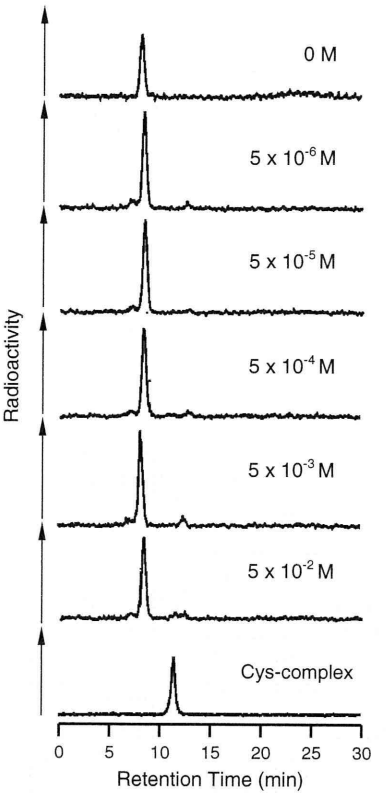

Figure 7. SE-HPLC profiles of ^{99m}Tc-C_3(BHam)$_2$-HSA after incubation with L-cysteine for 1 h at 37 °C.

of ^{99m}Tc-C_3(BHam)$_2$-COOH (Rt = 7 min) (Figure 4(A)). In the analysis by CAEP, almost all radioactivity existed at the origin different from the site where the radioactivity of $^{99m}TcO_4^-$ and C_3(BHam)$_2$-COOH was detected, suggesting the production of ^{99m}Tc-C_3(BHam)$_2$-TFP (Figure 4(B)). The recovery rate of radioactivity was ca. 50% after purification by Sep-Pak, and the rest remained in the Sep-Pak column.

We performed by gel filtration chromatography after the conjugation of ^{99m}Tc-C_3(BHam)$_2$-TFP with HSA and analyzed the radioactivity eluted from the gel filtration column by SE-HPLC and CAEP (Figure 5). In the SE-HPLC analysis, the peaks of radioactivity at retention times of 7 (dimer) and 8 min (monomer) corresponded with the peaks of UV (254 nm) for unmodified HSA (Figure 7(A, B)). In the CAEP analysis, over 95% of radioactivity was detected at the same position as HSA stained with Ponceau 3R (Figure 5(C, D)). The radiochemical yield and purity were ca. 75% and >95%, respectively. The results suggested that C_3(BHam)$_2$-COOH may serve as a BCA for the labeling of polypeptides with ^{99m}Tc.

Next, we tested the stability of ^{99m}Tc-C_3(BHam)$_2$-HSA in PB or murine plasma at 37 °C by CAEP (Figure 6). The amount of radioactivity bound to HSA was over 95% until 6 h. We also

Table 1. Biodistribution of radioactivity after injection of ^{99m}Tc-C_3(BHam)$_2$-HSA in mice

	Percentage of injected dose per tissue				
Tissue	5 min	10 min	30 min	1 h	3 h
Blood[a]	35.60	32.92	31.42	27.94	19.54
	(2.69)	(2.01)	(1.47)	(3.17)	(2.62)
Liver	7.39	8.72	8.07	7.28	5.68
	(1.60)	(1.09)	(0.70)	(1.07)	(0.62)
Kidney	1.68	1.47	1.88	1.76	1.31
	(0.41)	(0.29)	(0.21)	(0.29)	(0.08)
Intestine	2.04	2.62	4.81	7.27	11.56
	(0.45)	(0.35)	(0.39)	(1.18)	(0.78)
Spleen	0.33	0.35	0.32	0.30	0.21
	(0.01)	(0.05)	(0.06)	(0.04)	(0.03)
Stomach	0.51	0.63	1.00	1.02	0.95
	(0.10)	(0.02)	(0.24)	(0.10)	(0.11)
Lung	3.50	3.65	2.62	3.13	1.80
	(0.47)	(0.72)	(0.38)	(0.44)	(0.52)

Each value represents the mean (SD) for four to five animals.
[a]Expressed as% injected dose per gram.

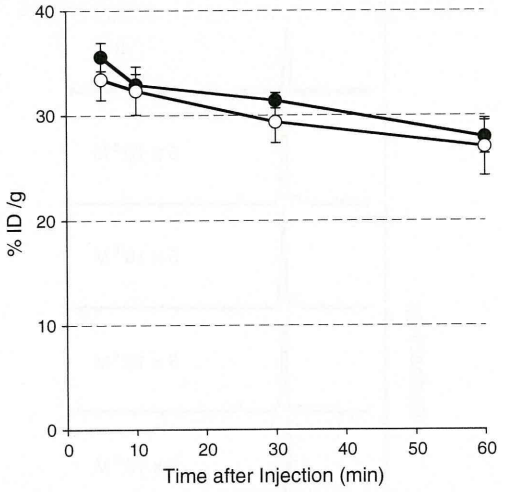

Figure 8. Blood clearance of radioactivity after injection of ^{99m}Tc-C_3(BHam)$_2$-HSA (●) and ^{125}I-HSA (○) in mice.

analyzed the radioactivity of ^{99m}Tc-C_3(BHam)$_2$-HSA by SE-HPLC after incubation with excess L-cysteine (Figure 7). No marked change in the peak of radioactivity was observed at 5×10^{-5} M, 5×10^{-4} M, 5×10^{-3} M, or 5×10^{-2} M of L-cysteine. These results suggested that ^{99m}Tc stably binds to HSA via C_3(BHam)$_2$-COOH.

Furthermore, we determined the biodistribution of radioactivity after the injection of ^{99m}Tc-C_3(BHam)$_2$-HSA into mice (Table 1). At 5-min postinjection, 36% ID/g was observed in the blood, and at 180 min, 20%ID/g. The profile of radioactivity was similar to that for ^{125}I-HSA (Figure 8). The results suggested that ^{99m}Tc-C_3(BHam)$_2$-HSA may reflect the pharmacokinetics of HSA without the dissociation of ^{99m}Tc from HSA, and in addition, C_3(BHam)$_2$-COOH serves as a BCA, which can give stable ^{99m}Tc-labeled polypeptides. As no marked increase in radioactivity was detected in the stomach and lungs, the reoxidation to $^{99m}TcO_4^-$ or production of ^{99m}Tc-colloid did not seem to occur, supporting the notion that C_3(BHam)$_2$-COOH serves as a BCA that produces stable ^{99m}Tc-labeled polypeptides *in vivo*.

When radiolabeled polypeptides were administered *in vivo*, persistently high levels of radioactivity were observed in the liver and kidney where catabolism of the parent proteins and peptides occurs, which compromises the diagnostic accuracy of these radiopharmaceuticals. Previous investigations regarding the radiometabolites produced in the liver and kidney indicated that slow elimination rates are responsible for the persistent localization of radioactivity in the lysosomal compartment of hepatic and renal cells.[31–34] Several recent studies suggested that an experimental system using NGA, which is incorporated by hepatic parenchymal cells via receptor-mediated endocytosis immediately after its administration, is suitable for investigating radiometabolites formed in the liver.[31–34] To investigate the pharmacokinetics of the radiometabolites produced in the metabolic tissues after the injection of ^{99m}Tc-labeled polypeptides by using C_3(BHam)$_2$-COOH as a BCA, NGA was selected as a model polypeptide, ^{99m}Tc-C_3(BHam)$_2$-NGA was prepared, and the biodistribution in mice was evaluated. The biodistribution of radioactivity after the injection of ^{99m}Tc-C_3(BHam)$_2$-NGA is summarized in Table 2. At 5-min postinjection, more than 89% of the radioactivity was accumulated in the liver. The radioactivity was rapidly eliminated from the liver by hepatobiliary excretion. At 6-h postinjection, the radioactivity retained in the liver was just 7% of the injected dose. No marked accumulation in the blood or the other tissues was observed.

We compared the clearance of ^{99m}Tc-C_3(BHam)$_2$-NGA from the liver with that of ^{99m}Tc-(HYNIC-NGA)(tricine)$_2$ (Figure 9).[17] Radioactivity in the liver cleared faster after the injection of ^{99m}Tc-C_3(BHam)$_2$-NGA than that of ^{99m}Tc-(HYNIC-NGA)(tricine)$_2$, indicating that ^{99m}Tc-labeled polypeptides prepared with C_3(BHam)$_2$-COOH produce radiometabolites, which show rapid elimination from the liver. We have not determined the radiometabolites produced in the liver after the injection of ^{99m}Tc-labeled polypeptides by using C_3(BHam)$_2$-COOH as a BCA. Previous studies using ^{111}In-labeled NGAs with cDTPA or SCN-Bz-EDTA or ^{99m}Tc-HYNIC-NGA showed that radiolabeled NGAs generated lysine-adducts ([^{111}In]

Table 2. Biodistribution of radioactivity after injection of ^{99m}Tc-C_3(BHam)$_2$-NGA in mice

	Percentage of injected dose per tissue					
Tissue	5 min	10 min	30 min	1 h	3 h	6 h
Blood[a]	1.35	0.89	1.84	1.49	0.98	0.75
	(0.28)	(0.39)	(0.39)	(0.48)	(0.42)	(0.31)
Liver	89.43	80.52	59.96	32.66	14.64	7.12
	(4.15)	(7.71)	(2.79)	(2.87)	(3.05)	(0.62)
Kidney	0.36	0.33	0.45	0.53	0.50	0.36
	(0.11)	(0.04)	(0.09)	(0.13)	(0.13)	(0.01)
Intestine	0.93	2.28	22.33	43.66	62.44	27.74
	(0.03)	(0.34)	(1.87)	(6.16)	(4.05)	(11.02)
Spleen	0.19	0.16	0.18	0.14	0.13	0.11
	(0.07)	(0.03)	(0.03)	(0.01)	(0.06)	(0.03)
Stomach	0.41	0.51	0.58	0.74	0.51	0.27
	(0.13)	(0.11)	(0.16)	(0.28)	(0.22)	(0.09)
Lung	0.24	0.17	0.19	0.21	0.21	0.12
	(0.13)	(0.03)	(0.05)	(0.03)	(0.01)	(0.03)

Each value represents the mean (SD) for five to eight animals.
[a]Expressed as% injected dose per gram.

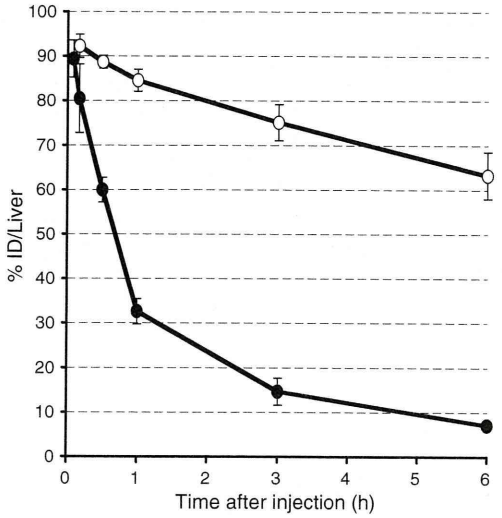

Figure 9. Elimination of radioactivity from the liver after injection of ^{99m}Tc-C_3(BHam)$_2$-NGA (•) and ^{99m}Tc-(HYNIC-NGA)(tricine)$_2$ (○) (data from Abrams *et al.*[16]) in normal mice.

DTPA-lysine, [^{111}In]SCN-Bz-EDTA-lysine, and ^{99m}Tc-HYNIC-lysine) as the major final radiometabolites in murine hepatocytes.[31,32,35,36] As ^{99m}Tc-C_3(BHam)$_2$-COOH was also conjugated to the ε-amine residues of NGA, it was speculated that a lysine adduct of ^{99m}Tc-C_3(BHam)$_2$ may be produced in the liver as the final radiometabolite. The rapid elimination of radioactivity after the injection of ^{99m}Tc-C_3(BHam)$_2$-NGA may reflect the rapid clearance of the final radiometabolites from the lysosomal compartment of hepatocytes. Although ^{99m}Tc-labeled polypeptides showed high and persistent levels of radioactivity in the liver and kidney, the present results observed for ^{99m}Tc-C_3(BHam)$_2$-NGA suggested that C_3(BHam)$_2$-COOH is a useful BCA for labeling with ^{99m}Tc to reduce the non-specific accumulation in the liver observed for ^{99m}Tc-HYNIC-polypeptides. Low molecular weight polypeptides including single-chain Fv fragments, diabodies, affibodies, minibodies, and bioactive small peptides are attractive scaffolds of ^{99m}Tc-labeled probes for targeted imaging because of the pharmacokinetic properties of these molecules. As ^{99m}Tc has an appropriate half-life to label such polypeptides, the application of C_3(BHam)$_2$-COOH as a BCA to low molecular weight polypeptides is expected in the future.

In conclusion, we successfully designed and synthesized C_3(BHam)$_2$-COOH as a new BCA for ^{99m}Tc labeling of polypeptides. C_3(BHam)$_2$-COOH formed a stable ^{99m}Tc complex and enabled us to prepare ^{99m}Tc-labeled polypeptides by using a TFP active ester of C_3(BHam)$_2$-COOH. ^{99m}Tc-C_3(BHam)$_2$-HSA existed stably in murine plasma and an excess of L-cysteine without any dissociation of ^{99m}Tc from polypeptides. Furthermore, as the blood clearance of ^{99m}Tc-C_3(BHam)$_2$-HSA in mice was similar to that of ^{125}I-HSA, C_3(BHam)$_2$-COOH retained stable binding between ^{99m}Tc and polypeptide *in vivo*. When we determined radioactivity after the injection of ^{99m}Tc-C_3(BHam)$_2$-NGA into mice, we found high liver uptake early on and rapid clearance from the liver, indicating that C_3(BHam)$_2$-COOH did not affect the pharmacokinetics of polypeptides *in vivo* and gave radiometabolites which showed rapid elimination from the liver. Such characteristics would render C_3(BHam)$_2$-COOH attractive as a new BCA for ^{99m}Tc labeling of polypeptides.

Acknowledgements

The study was supported by the Funding Program for Next Generation World-Leading Researchers (NEXT Program), and a Grant-in-aid for Young Scientists and Exploratory Research from the Ministry of Education, Culture, Sports, Science and Technology, Japan.

Conflict of Interest

The authors did not report any conflict of interest.

References

[1] G. Malviya, C. D'Alessandria, E. Bonanno, V. Vexler, R. Massari, C. Trotta, F. Scopinaro, R. Dierckx, A. Signore, *J. Nucl. Med.* **2009**, *50*, 1683–1691.
[2] M. D. Bartholoma, A. S. Louie, J. F. Valliant, J. Zubieta, *Chem. Rev.* **2010**, *110*, 2903–2920.
[3] S. M. Okarvi, *Med. Res. Rev.* **2004**, *24*, 357–397.
[4] A. J. Fischman, J. W. Babich, H. D. Strauss, *J. Nucl. Med.* **1993**, *34*, 2253–2263.
[5] H. Wållberg, A. Orlova, M. Altai, S. J. Hosseinimehr, C. Widström, J. Malmberg, S. Ståhl, V. Tolmachev, *J. Nucl. Med.* **2011**, *52*, 461–469.
[6] L. Li, D. Crow, F. Turatti, J. R. Bading, A. L. Anderson, E. Poku, P. J. Yazaki, J. Carmichael, D. Leong, M. P. Wheatcroft, A. A. Raubitschek, P. J. Hudson, D. Colcher, J. E. Shively, *Bioconj. Chem.* **2011**, *22*, 709–716.
[7] S. Hoppmann, Z. Miao, S. Liu, H. Liu, G. Ren, A. Bao, Z. Cheng, *Bioconj. Chem.* **2011**, *22*, 413–421.
[8] L. Li, F. Turatti, D. Crow, J. R. Bading, A. L. Anderson, E. Poku, P. J. Yazaki, L. E. Williams, D. Tamvakis, P. Sanders, D. Leong, A. Raubitschek, P. J. Hudson, D. Colcher, J. E. Shively, *J. Nucl. Med.* **2010**, *51*, 1139–1146.
[9] E. J. Lepin, J. V. Leyton, Y. Zhou, T. Olafsen, F. B. Salazar, K. E. McCabe, S. Hahm, J. D. Marks, R. E. Reiter, A. M. Wu, *Eur. J. Nucl. Med. Mol. Imaging* **2010**, *37*, 1529–1538.
[10] T. Olafsen, D. Betting, V. E. Kenanova, F. B. Salazar, P. Clarke, J. Said, A. A. Raubitschek, J. M. Timmerman, A. M. Wu, *J. Nucl. Med.* **2009**, *50*, 1500–1508.
[11] Y. Arano, *Ann. Nucl. Med.* **2002**, *16*, 79–93.
[12] S. Liu, D. Edwards, *Chem. Rev.* **1999**, *99*, 2236–2268.
[13] A. R. Fritzberg, P. G. Abrams, P. L. Beaumier, S. Kasina, A. C. Morgan, T. N. Rao, J. M. Reno, J. A. Sanderson, A. Srinivasan, D. S. Wilbur, J. L. Vanderheyden, *Proc. Natl. Acad. Sci. U.S.A.* **1988**, *85*, 4025–4029.
[14] S. Liu, D. S. Edwards, R. J. Looby, M. J. Poirier, M. Rajopadhye, J. P. Bourque, T. R. Carroll, *Bioconjug. Chem.* **1996**, *7*, 196–202.
[15] R. W. Weber, R. H. Boutin, M. A. Nedelman, J. Lister-James, R. T. Dean, *Bioconjug. Chem.* **1990**, *1*, 431–437.
[16] M. J. Abrams, M. Juweid, C. I. ten Kate, D. A. Schwartz, M. M. Hauser, F. E. Gaul, A. J. Fuccello, R. H. Rubin, H. W. Strauss, A. J. Fischman, *J. Nucl. Med.* **1990**, *31*, 2022–2028.
[17] M. Ono, Y. Arano, T. Uehara, Y. Fujioka, K. Ogawa, S. Namba, T. Mukai, M. Nakayama, H. Saji, *Bioconjug. Chem.* **1999**, *10*, 386–394.
[18] A. Purohit, S. Liu, D. Casebier, D. S. Edwards, *Bioconjug. Chem.* **2003**, *14*, 720–727.
[19] A. Purohit, S. Liu, C. E. Ellars, D. Casebier, S. B. Haber, D. S. Edwards, *Bioconjug. Chem.* **2004**, *15*, 728–737.
[20] M. Nakayama, H. Saigo, E. Kai, A. Koda, H. Ozeki, K. Harada, A. Sugii, S. Tomiguchi, A. Kojima, M. Hara, R. Kinoshita, M. Takahashi, *Nucl. Med. Commun.* **1992**, *13*, 445–449.
[21] M. Nakayama, H. Saigo, A. Koda, K. Ozeki, K. Harada, A. Sugii, S. Tomiguchi, A. Kojima, M. Hara, R. Nakasima, Y. Ohyama, M. Takahashi, J. Takata, Y. Karube, *Appl. Radiat. Isot.* **1994**, *45*, 735–740.
[22] M. Nakayama, L. C. Xu, Y. Koga, K. Harada, A. Sugii, M. Nakanama, S. Tomiguchi, A. Kojima, Y. Ohyama, M. Takahashi, I. Okabayashi, *Appl. Radiat. Isot.* **1997**, *48*, 571–577.
[23] L. C. Xu, M. Nakayama, K. Harada, A. Kuniyasu, H. Nakayama, S. Tomiguchi, A. Kojima, M. Takahashi, M. Ono, Y. Arano, H. Saji, Z. Yao, H. Sakahara, J. Konishi, Y. Imagawa, *Bioconjug. Chem.* **1999**, *10*, 9–17.

[24] L. C. Xu, M. Nakayama, K. Harada, H. Nakayama, S. Tomiguchi, A. Kojima, M. Takahashi, Y. Arano, *Nucl. Med. Biol.* **1998**, *25*, 295–303.
[25] K. Thipyapong, T. Uehara, Y. Tooyama, H. Braband, R. Alberto, Y. Arano, *Inorg. Chem.* **2011**, *50*, 992–998.
[26] K. Verbeke, K. Snauwaert, B. Cleynhens, W. Scheers, A. Verbruggen, *Nucl. Med. Biol.* **2000**, *27*, 769–779.
[27] Y. M. Zhang, N. Liu, Z. H. Zhu, M. Rusckowski, D. J. Hnatowich, *Eur. J. Nucl. Med.* **2000**, *27*, 1700–1707.
[28] Y. C. Lee, C. P. Stowell, M. J. Krantz, *Biochemistry* **1976**, *15*, 3956–3963.
[29] C. P. Stowell, Y. C. Lee, *Biochemistry* **1980**, *19*, 4899–4904.
[30] G. W. M. Visser, M. Gerretsen, J. D. M. Herscheid, G. B. Snow, G. V. Dongen, *J. Nucl. Med.* **1993**, *34*, 1953–1963.
[31] Y. Arano, T. Mukai, T. Uezono, K. Wakisaka, H. Motonari, H. Akizawa, Y. Taoka, A. Yokoyama, *J. Nucl. Med.* **1994**, *35*, 890–898.
[32] Y. Arano, T. Mukai, H. Akizawa, T. Uezono, H. Motonari, K. Wakisaka, C. Kairiyama, A. Yokoyama, *Nucl. Med. Biol.* **1995**, *22*, 555–564.
[33] T. Mukai, Y. Arano, K. Nishida, H. Sasaki, J. Nakamura, H. Saji, A. Yokoyama, *Nucl. Med. Biol.* **1998**, *25*, 31–36.
[34] T. Mukai, Y. Arano, K. Nishida, H. Sasaki, H. Akizawa, K. Ogawa, M. Ono, H. Saji, J. Nakamura, *Nucl. Med. Biol.* **1999**, *26*, 281–289.
[35] J. R. Duncan, M. J. Welch, *J. Nucl. Med.* **1993**, *34*, 1728–1738.
[36] B. E. Rogers, F. N. Franano, J. R. Duncan, W. B. Edwards, C. J. Anderson, J. M. Connett, M. J. Welch, *Cancer Res.* **1995**, *55*, 5714s–5720s.

ACS Medicinal Chemistry Letters

Letter

pubs.acs.org/acsmedchemlett

^{18}F-Labeled Phenyldiazenyl Benzothiazole for in Vivo Imaging of Neurofibrillary Tangles in Alzheimer's Disease Brains

Kenji Matsumura,[†] Masahiro Ono,*[,†] Hiroyuki Kimura,[†] Masashi Ueda,[†] Yuji Nakamoto,[‡] Kaori Togashi,[‡] Yoko Okamoto,[§] Masafumi Ihara,[§] Ryosuke Takahashi,[§] and Hideo Saji[†]

[†]Department of Patho-Functional Bioanalysis, Graduate School of Pharmaceutical Sciences, Kyoto University, 46-29 Yoshida Shimoadachi-cho, Sakyo-ku, Kyoto 606-8501, Japan

[‡]Department of Diagnostic Imaging and Nuclear Medicine, Graduate School of Medicine, Kyoto University, 54 Shogoin-kawaharacho, Sakyo-ku, Kyoto 606-8507, Japan

[§]Department of Neurology, Graduate School of Medicine, Kyoto University, 54 Shogoin-kawaharacho, Sakyo-ku, Kyoto 606-8507, Japan

S *Supporting Information*

ABSTRACT: We synthesized and evaluated (*E*)-4-((6-(2-(2-(2-fluoroethoxy)ethoxy)ethoxy)benzo[*d*]thiazol-2-yl)-diazenyl)-*N*,*N*-dimethylaniline (FPPDB) as a probe for the imaging of neurofibrillary tangles (NFTs) in patients with Alzheimer's disease (AD). In assays using thioflavin S (ThS) as a competitive ligand, FPPDB competed with ThS well and showed high affinity for both tau and Aβ_{1-42} aggregates (K_i = 13.0 and 20.0 nM, respectively). The results of saturation binding assays also verified that FPPDB bound to both tau and Aβ_{1-42} aggregates with high affinity (K_d = 44.8 nM and B_{max} = 45.8 pmol/nmol protein for tau aggregates and K_d = 45.4 nM and B_{max} = 38.9 pmol/nmol protein for Aβ_{1-42} aggregates). Furthermore, [^{18}F]FPPDB substantially labeled NFTs and senile plaques in AD brain sections but not control brain sections. In biodistribution experiments using normal mice, [^{18}F]FPPDB displayed higher uptake (4.28% ID/g at 2 min postinjection) into and washout (2.53% ID/g at 60 min postinjection) from the brain with time. On the basis of the chemical structure of FPPDB, further increases in selective binding to tau aggregates may lead to the development of more useful probes for the imaging of NFTs in AD brains.

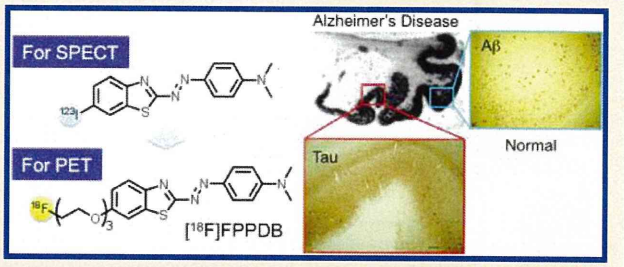

KEYWORDS: *Alzheimer's disease (AD), neurofibrillary tangles (NFTs), imaging, benzothiazole, PET*

Alzheimer's disease (AD) is a progressive neurodegenerative brain disorder associated with cognitive decline, disorientation, and language impairment and is characterized by the presence of senile plaques (SPs) composed of β-amyloid (Aβ) peptides and neurofibrillary tangles (NFTs) composed of hyperphosphorylated tau protein.[1] At present, the clinical diagnosis of AD depends on medical history and neuropsychological findings, and the early cognitive and behavioral symptoms of AD are often indistinguishable from normal signs of aging. Because a definite diagnosis of AD is based on the postmortem histopathological examination of SPs and NFTs, useful methods of evaluating the histopathological changes in vivo are strongly needed. The formation of SPs is considered an initial manifestation of AD. Therefore, considerable effort has focused on the development of imaging probes targeting SPs for positron emission tomography (PET) and single photon emission computed tomography (SPECT). Among them, PET/SPECT probes such as IMPY,[2] SB-13,[3] PIB,[4] AZD2184,[5] FDDNP,[6] BAY94-9172,[7] AV-45,[8] and GE-067[9] have been tested clinically and demonstrated the potential utility of the in vivo imaging of SPs in the brain. Many other compounds with structural similarities have also been reported.

Since the accumulation of NFTs is highly correlated with symptoms of AD[10,11] and the detection of NFTs in the brain should lead to the early diagnosis of AD and the evaluation of severity and staging, the development of NFT-selective binding probes is needed. However, there have been few reports on the development of PET/SPECT imaging probes targeting NFTs.

A previous paper has reported quinoline and benzimidazole derivatives as candidate probes for the imaging of NFTs in AD brains.[12,13] However, these derivatives showed affinity for both NFTs and SPs, suggesting that they may not be NFT-selective tracers. Therefore, to investigate the selective binding affinity for both NFTs and SPs, we recently developed radioiodinated compounds based on another chemical structure, a phenyldiazenyl benzothiazole (PDB) scaffold (Figure 1).[14] All of the PDB derivatives displayed high affinity for tau aggregates. PDB-

Received: September 23, 2011
Accepted: November 29, 2011
Published: December 1, 2011

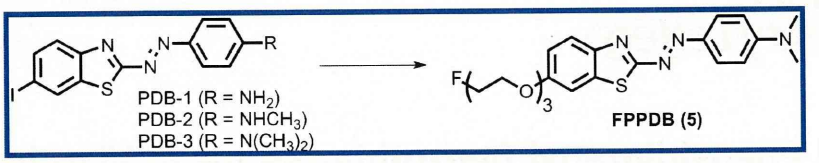

Figure 1. Chemical structure of iodinated and fluoro-pegylated PDB derivatives.

Scheme 1. [a]

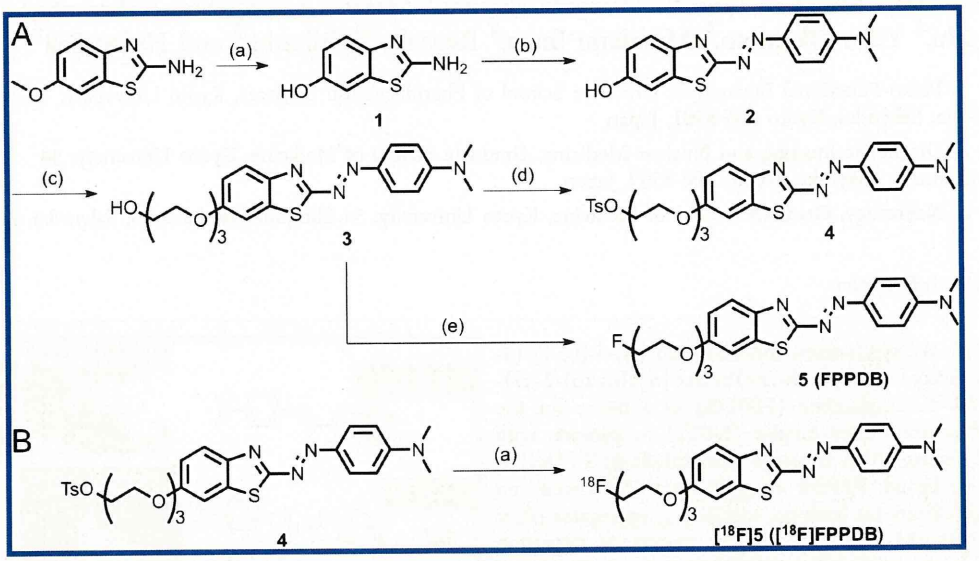

[a](A) Reagents and conditions: (a) HBr, reflux. (b) *N,N*-Dimethylaniline, $NaNO_2$, 50% H_2SO_4, concentrated HCl, 0 °C. (c) 2-[2-(2-Chloroethoxy)ethoxy]ethanol, K_2CO_3, DMF, 105 °C. (d) Tosyl chloride, pyridine. (e) Diethylamino sulfur trifluoride, 1,2-dimethoxyethane. (B) Reagents and conditions: (a) $^{18}F^-$, Kryptofix222, K_2CO_3, acetonitrile, 100 °C, 5 min.

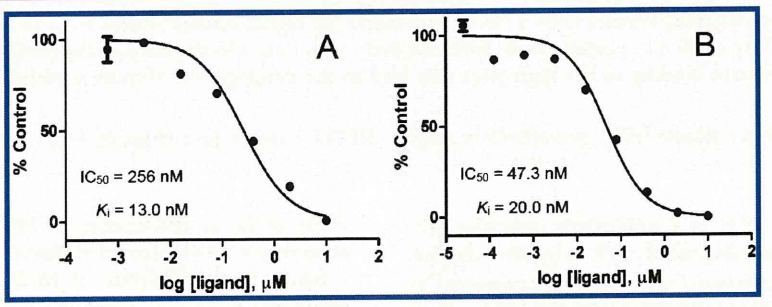

Figure 2. Inhibition curves for the binding of ThS to tau (A) and $A\beta_{1-42}$ (B) aggregates using FPPDB as a test compound.

3, with a dimethylamino group at position 4 of the phenyl group, showed the highest affinity (17.2-fold that for $A\beta_{1-42}$ aggregates), indicating it to be a tracer with greater selective binding to tau aggregates than the quinoline and benzimidazole derivatives reported previously. However, ^{125}I-labeled PDB derivatives showed a relatively low uptake into and slow washout from the brain, suggesting high nonspecific binding, which would contribute to a high level of background noise. Since the slow washout of [^{125}I]PDB derivatives in normal mice prevents imaging in vivo, the improved property of the PDB derivatives should make them better candidates for the study of tau aggregates.

Previous studies regarding uptake into and clearance from the brain points to high lipophilicity as one of the reasons for a slow washout.[15,16] We then planned to develop a novel PDB derivative with less lipophilicity by substituting iodine, which increases the lipophilicity of a compound, with fluorine for the preparation of PET tracers. Recent reports have introduced a new approach, fluoro-pegylation (FPEG) of the core structure, to labeling with ^{18}F.[7,17,18] Because this approach offers a simple and easy way to incorporate ^{18}F without any increase in lipophilicity, we selected FPEG for ^{18}F-labeling of the PDB scaffold. In the present study, we designed and synthesized a novel fluorinated ligand, (*E*)-4-((6-(2-(2-(2-fluoroethoxy)-ethoxy)ethoxy)benzo[*d*]thiazol-2-yl)diazenyl)-*N,N*-dimethylaniline (FPPDB, Figure 1) with a fluoro-polyethylene glycol side chain instead of iodine at position 6 of PDB-3, and evaluated its potential as a probe for the imaging NFTs in the brains in vivo.

A new ligand, FPPDB, was prepared as outlined in Scheme 1A. A methoxy group of 2-amino-6-methoxybenzothiazole was converted to a hydroxy group using a HBr solution, which afforded **1** in a yield of 71.0%. To obtain the backbone

dx.doi.org/10.1021/ml200230e | *ACS Med. Chem. Lett.* 2012, 3, 58–62

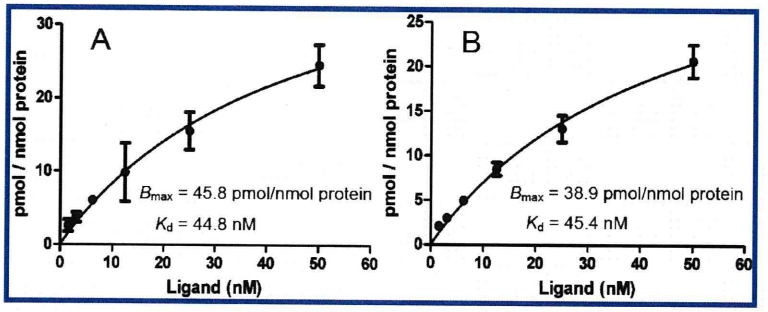

Figure 3. Saturation curves of [^{18}F]FPPDB for tau (A) and Aβ_{1-42} (B) aggregates.

structure of PDB, we used a diazo coupling reaction with *N,N*-dimethylaniline to afford **2**. Thereafter, 2-[2-(2-chloroethoxy)-ethoxy]ethanol was coupled with the OH group of **2** to obtain **3**. Fluorination of **3** to prepare **5** was achieved using diethylamino sulfur trifluoride (DAST). ^{18}F-labeling of **5** was performed on a tosyl precursor (**4**) undergoing a nucleophilic displacement reaction with the fluoride anion (Scheme 1B). Radiolabeling with ^{18}F was successfully performed on the precursor to generate [^{18}F]**5** ([^{18}F]FPPDB) with a radiochemical yield of 35% and radiochemical purity >99%. The identity of [^{18}F]FPPDB was verified by a comparison of retention time with the nonradioactive compound.

To evaluate the affinity of FPPDB for both tau aggregates and Aβ_{1-42} aggregates, an assay using thioflavin-S (ThS) as a competitive ligand was carried out. Similarly to iodinated PDB derivatives reported previously, FPPDB competed well with ThS to bind to tau aggregates (Figure 2A). The K_i value of FPPDB for tau aggregates was estimated at 13.0 nM. Although FPPDB exhibited significantly lower affinity than PDB-3 (K_i = 0.48 nM), it still maintained high enough affinity for tau aggregates to image NFTs. Because both tau and Aβ_{1-42} aggregates possess a β-sheet structure, it would be important to examine the selectivity of FPPDB. To this end, we determined the affinity of FPPDB for Aβ_{1-42} aggregates using a competitive inhibition assay with ThS. FPPDB also inhibited the binding of ThS to Aβ_{1-42} aggregates (Figure 2B), the K_i value being 20.0 nM. The ratio of the K_i values for tau and Aβ_{1-42} aggregates was 1.54. As compared to PDB-3 (ratio of 17.2),[14] FPPDB exhibited less selectivity between tau and Aβ_{1-42} aggregates. The results suggest that the substituted group at position 6 in the PDB scaffold plays an important role in the binding to β-sheet structures in both tau and Aβ_{1-42} aggregates. The concentration of tau aggregates (~150−300 pmol mg^{-1} of wet tissue) was reported to be higher than that of Aβ aggregates (~9 pmol mg^{-1} of wet tissue) in the frontal and temporal cortices in late-stage AD,[19,20] so it may be possible for [^{18}F]FPPDB to show contrast between NFTs and SPs in these areas in vivo. However, to diagnose AD in the early stages, probes with much higher NFT selectivity will be needed.

In competitive inhibition assays, FPPDB competed with ThS to bind to both tau and Aβ_{1-42} aggregates. To verify that FPPDB bound to these aggregates directly, saturation binding assays of [^{18}F]FPPDB to these aggregates were carried out (Figure 3). A Scatchard analysis revealed the K_d value and B_{max} of FPPDB for both tau and Aβ_{1-42} aggregates to be almost equal (K_d = 44.8 nM and B_{max} = 45.8 pmol/nmol tau protein for tau aggregates and K_d = 45.4 nM and B_{max} = 38.9 pmol/nmol Aβ_{1-42} protein for Aβ_{1-42} aggregates). This result showed that FPPDB had almost equal affinity for tau and Aβ_{1-42} aggregates, which was reflected the K_i values of FPPDB for both aggregates in the competitive inhibition assays using ThS.

[^{18}F]FPPDB was investigated for its affinity for NFTs in vitro by autoradiography in human AD brain sections (Figure 4).

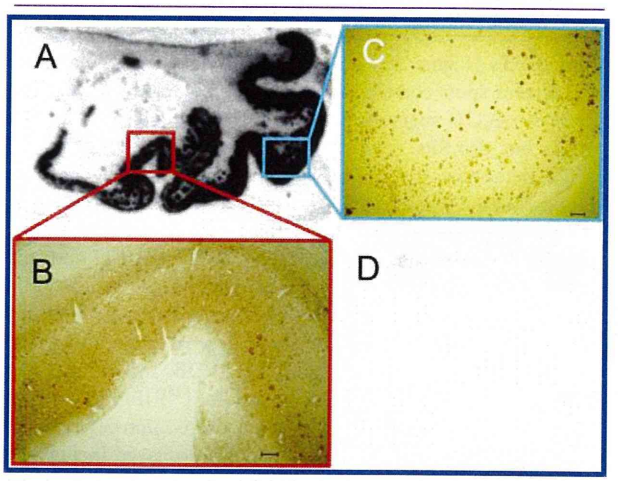

Figure 4. Autoradiogram of [^{18}F]FPPDB (A) and immunohistochemical staining with antibodies against hyperphosphorylated tau (B) and Aβ_{1-42} (C) in brain sections from the same patient. Autoradiogram of a control brain (D). Bars indicate 200 μm.

Autoradiographic images of [^{18}F]FPPDB showed the accumulation of radioactivity in the AD brain sections with little nonspecific binding in white matter (Figure 4A). The accumulation corresponded with the results of immunohistochemical staining with both the anti phosphorylated tau antibody (AT8) and the anti Aβ_{1-42} antibody (BC05) (Figure 4B,C, respectively). Conversely, [^{18}F]FPPDB showed almost no accumulation in normal human brain sections (Figure 4D). These results suggested that [^{18}F]FPPDB had enough affinity to label NFTs in AD brain sections, although its affinity for tau aggregates was lower than that of iodinated PDB derivatives. However, the results also indicated that [^{18}F]FPPDB did not possess enough selectivity for NFTs to show high contrast between NFTs and SPs in an autoradiographic study, similarly to the iodinated PDB derivatives reported previously.

To further confirm the affinity of FPPDB for NFTs and SPs in the AD brain, fluorescent staining was carried out using brain sections from the same AD patient (Figure 5). Numerous fluorescent spots were detected in the entorhinal cortex of AD brain sections (Figure 5A,C) as reflected by the high affinity for recombinant tau and Aβ_{1-42} aggregates in both competitive inhibition and saturation binding assays in vitro. ThS stained

dx.doi.org/10.1021/ml200230e | ACS Med. Chem. Lett. 2012, 3, 58–62

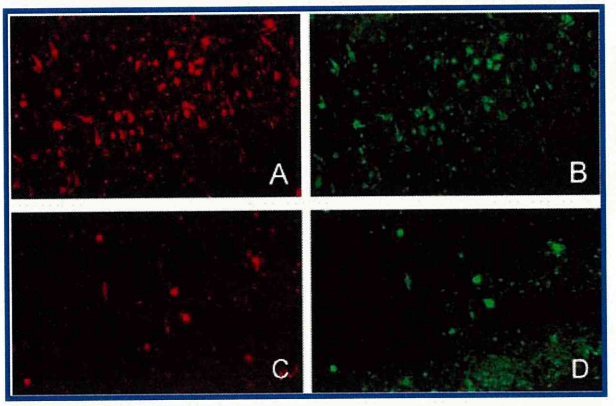

Figure 5. Fluorescent staining with FPPDB (A and C) and ThS (B and D) in the entorhinal cortex of AD brain sections. Many NFTs were clearly stained with FPPDB (A) and ThS (B). SPs were also stained with FPPDB (C) and ThS (D).

both NFTs (Figure 5B) and SPs (Figure 5D) clearly, and the fluorescent spots corresponded to those obtained with FPPDB (Figure 5A,C), suggesting that FPPDB bound to not only NFTs but also SPs.

To determine the uptake of [^{18}F]FPPDB in the brain, a biodistribution experiment was performed in normal mice (Table 1). [^{18}F]FPPDB displayed high uptake (4.28% ID/g) at 2 min postinjection, sufficient for PET imaging, and the radioactivity in the brain cleared with time. At 60 min postinjection, the uptake was 2.53% ID/g, indicating a relatively fast washout from the brain. Since normal brain tissue has neither NFTs nor SPs to trap [^{18}F]FPPDB, the radioactivity should wash out quite rapidly. Therefore, [^{18}F]FPPDB's rapid clearance from normal brain makes it more appropriate as an imaging agent for AD brain. [^{125}I]PDB-3 displayed less uptake into and a slower washout from the brain (0.94 and 2.89% ID/g at 2 and 60 min postinjection, respectively) than [^{18}F]-FPPDB.[14] The improved pharmacokinetics of [^{18}F]FPPDB were achieved by replacing iodine with a fluoro-pegylated group at position 6. The log *P* value of [^{18}F]FPPDB and [^{125}I]PDB-3 was 2.05 and 3.84, respectively, suggesting that [^{18}F]FPPDB is less lipophilic than [^{125}I]PDB-3. Although lipophilicity is just one of the factors influencing the uptake of a compound into the brain, it may explain in the favorable pharmacokinetics of [^{18}F]FPPDB. However, as compared with several Aβ imaging probes under clinical study such as [^{18}F]BAY94-9172[7] and [^{18}F]AV-45,[8] [^{18}F]FPPDB's uptake into and washout from the brain were not particularly satisfactory. The replacement of the dimethylamino group of [^{18}F]FPPDB with a less lipophilic group may lead to the development of more promising probes for diagnosing AD. Because defluorination, as reflected by the uptake of [^{18}F]FPPDB into bone, was low (1.82−1.92% ID/g), interference with the imaging is expected to be relatively minor. [^{18}F]FPPDB was cleared from plasma by not only the hepatobiliary system (20.2% ID/g in the liver at 2 min postinjection) but the renal system (13.9% ID/g in the kidney at 2 min postinjection). The hepatobiliary excretion to the intestines was also rather fast, and radioactivity was observed to accumulate within the intestine at later time points (22.9% ID/g at 60 min postinjection).

In conclusion, we designed, synthesized, and evaluated a PDB derivative, [^{18}F]FPPDB, as a novel PET imaging agent for diagnosing AD. In binding experiments in vitro, the derivative displayed high affinity for both tau and Aβ_{1-42} aggregates. NFTs and SPs were stained in experiments using autoradiography and fluorescent staining with AD brain sections, reflecting the results of the in vitro assays. Although FPPDB had lower selectivity for tau aggregates than PDB-3 in vitro, in biodistribution experiments using normal mice, [^{18}F]FPPDB had improved pharmacokinetics as compared with [^{125}I]PDB derivatives. Replacement of iodine with fluorine in the PDB scaffold was highly effective in improving the radioactive pharmacokinetics of [^{18}F]FPPDB in the brain. However, it resulted in a decrease in selective binding for tau aggregates. Further structural optimization based on the PDB scaffold, such as changing the position substituted in the fluoro-pegylated group or replacing the dimethylamino group with different groups to improve the affinity for tau aggregates may lead to the development of more useful probes for the in vivo imaging of NFTs in AD brains.

■ ASSOCIATED CONTENT

Supporting Information

Full experimental procedures and characterization data for all new compounds described in this study. This material is available free of charge via the Internet at http://pubs.acs.org.

Table 1. Biodistribution of Radioactivity after Injection of [^{18}F]FPPDB in Normal Mice[a]

	time after injection (min)			
tissue	2	10	30	60
blood	3.04 (0.40)	1.83 (0.82)	2.19 (0.75)	2.68 (0.63)
liver	20.2 (1.19)	19.3 (1.00)	13.1 (1.45)	9.32 (1.51)
kidney	13.9 (1.50)	7.67 (3.42)	5.08 (3.67)	4.00 (3.75)
intestine	2.94 (0.38)	4.99 (0.95)	14.4 (1.44)	22.9 (1.38)
spleen	3.47 (0.80)	3.41 (0.80)	2.71 (0.80)	2.14 (0.76)
pancreas	5.41 (0.69)	4.01 (1.03)	2.87 (0.63)	2.18 (0.67)
heart	7.45 (0.84)	4.14 (1.87)	3.05 (1.64)	2.62 (1.45)
lung	13.5 (3.51)	4.37 (4.60)	3.36 (3.70)	3.59 (3.18)
stomach[b]	1.11 (0.07)	1.42 (0.35)	2.69 (0.44)	3.37 (1.26)
brain	4.28 (0.45)	4.26 (0.37)	3.47 (0.54)	2.53 (0.54)
bone	1.88 (0.47)	1.82 (0.50)	1.82 (0.49)	1.92 (0.33)

[a]Each value represents the mean (SD) for five animals. [b]Expressed as % injected dose per organ.

dx.doi.org/10.1021/ml200230e | ACS Med. Chem. Lett. 2012, 3, 58–62

AUTHOR INFORMATION

Corresponding Author

*Tel: +81-75-753-4608. Fax: +81-75-753-4568. E-mail: ono@pharm.kyoto-u.ac.jp.

Funding

This study was supported by the Funding Program for Next Generation World-Leading Researchers (NEXT Program) and a Grant-in-aid for Young Scientists (A) and Exploratory Research from the Ministry of Education, Culture, Sports, Science and Technology, Japan.

Notes

The authors declare no competing financial interest.

ACKNOWLEDGMENTS

We thank Prof. Hiroshi Mori for kindly providing human tau cDNA for the in vitro binding assays.

REFERENCES

(1) Selkoe, D. J. Alzheimer's disease: Genes, proteins, and therapy. *Physiol. Rev.* **2001**, *81*, 741−766.

(2) Newberg, A. B.; Wintering, N. A.; Plossl, K.; Hochold, J.; Stabin, M. G.; Watson, M.; Skovronsky, D.; Clark, C. M.; Kung, M. P.; Kung, H. F. Safety, biodistribution, and dosimetry of ^{123}I-IMPY: a novel amyloid plaque-imaging agent for the diagnosis of Alzheimer's disease. *J. Nucl. Med.* **2006**, *47*, 748−754.

(3) Ono, M.; Wilson, A.; Nobrega, J.; Westaway, D.; Verhoeff, P.; Zhuang, Z. P.; Kung, M. P.; Kung, H. F. 11C-labeled stilbene derivatives as Aβ-aggregate-specific PET imaging agents for Alzheimer's disease. *Nucl. Med. Biol.* **2003**, *30*, 565−571.

(4) Klunk, W. E.; Engler, H.; Nordberg, A.; Wang, Y.; Blomqvist, G.; Holt, D. P.; Bergstrom, M.; Savitcheva, I.; Huang, G. F.; Estrada, S.; Ausen, B.; Debnath, M. L.; Barletta, J.; Price, J. C.; Sandell, J.; Lopresti, B. J.; Wall, A.; Koivisto, P.; Antoni, G.; Mathis, C. A.; Langstrom, B. Imaging brain amyloid in Alzheimer's disease with Pittsburgh Compound-B. *Ann. Neurol.* **2004**, *55*, 306−319.

(5) Johnson, A. E.; Jeppsson, F.; Sandell, J.; Wensbo, D.; Neelissen, J. A.; Jureus, A.; Strom, P.; Norman, H.; Farde, L.; Svensson, S. P. AZD2184: A radioligand for sensitive detection of β-amyloid deposits. *J. Neurochem.* **2009**, *108*, 1177−1186.

(6) Shoghi-Jadid, K.; Small, G. W.; Agdeppa, E. D.; Kepe, V.; Ercoli, L. M.; Siddarth, P.; Read, S.; Satyamurthy, N.; Petric, A.; Huang, S. C.; Barrio, J. R. Localization of neurofibrillary tangles and β-amyloid plaques in the brains of living patients with Alzheimer disease. *Am. J. Geriatr. Psychiatry* **2002**, *10*, 24−35.

(7) Zhang, W.; Oya, S.; Kung, M. P.; Hou, C.; Maier, D. L.; Kung, H. F. F-18 Polyethyleneglycol stilbenes as PET imaging agents targeting Aβ aggregates in the brain. *Nucl. Med. Biol.* **2005**, *32*, 799−809.

(8) Wong, D. F.; Rosenberg, P. B.; Zhou, Y.; Kumar, A.; Raymont, V.; Ravert, H. T.; Dannals, R. F.; Nandi, A.; Brasic, J. R.; Ye, W.; Hilton, J.; Lyketsos, C.; Kung, H. F.; Joshi, A. D.; Skovronsky, D. M.; Pontecorvo, M. J. In vivo imaging of amyloid deposition in Alzheimer disease using the radioligand ^{18}F-AV-45 (florbetapir F 18). *J. Nucl. Med.* **2010**, *51*, 913−920.

(9) Koole, M.; Lewis, D. M.; Buckley, C.; Nelissen, N.; Vandenbulcke, M.; Brooks, D. J.; Vandenberghe, R.; Van Laere, K. Whole-body biodistribution and radiation dosimetry of ^{18}F-GE067: A radioligand for in vivo brain amyloid imaging. *J. Nucl. Med.* **2009**, *50*, 818−822.

(10) Gomez-Isla, T.; Hollister, R.; West, H.; Mui, S.; Growdon, J. H.; Petersen, R. C.; Parisi, J. E.; Hyman, B. T. Neuronal loss correlates with but exceeds neurofibrillary tangles in Alzheimer's disease. *Ann. Neurol.* **1997**, *41*, 17−24.

(11) Arriagada, P. V.; Growdon, J. H.; Hedley-Whyte, E. T.; Hyman, B. T. Neurofibrillary tangles but not senile plaques parallel duration and severity of Alzheimer's disease. *Neurology* **1992**, *42*, 631−639.

(12) Okamura, N.; Suemoto, T.; Furumoto, S.; Suzuki, M.; Shimadzu, H.; Akatsu, H.; Yamamoto, T.; Fujiwara, H.; Nemoto, M.; Maruyama, M.; Arai, H.; Yanai, K.; Sawada, T.; Kudo, Y. Quinoline and benzimidazole derivatives: candidate probes for in vivo imaging of tau pathology in Alzheimer's disease. *J. Neurosci.* **2005**, *25*, 10857−10862.

(13) Fodero-Tavoletti, M. T.; Okamura, N.; Furumoto, S.; Mulligan, R. S.; Connor, A. R.; McLean, C. A.; Cao, D.; Rigopoulos, A.; Cartwright, G. A.; O'Keefe, G.; Gong, S.; Adlard, P. A.; Barnham, K. J.; Rowe, C. C.; Masters, C. L.; Kudo, Y.; Cappai, R.; Yanai, K.; Villemagne, V. L. ^{18}F-THK523: A novel in vivo tau imaging ligand for Alzheimer's disease. *Brain* **2011**, *134*, 1089−1100.

(14) Matsumura, K.; Ono, M.; Hayashi, S.; Kimura, H.; Okamoto, Y.; Ihara, M.; Takahashi, R.; Mori, H.; Saji, H. Phenyldiazenyl benzothiazole derivatives as probes for in vivo imaging of neurofibrillary tangles in Alzheimer's disease brains. *Med. Chem. Commun.* **2011**, *2*, 596−600.

(15) Cheng, Y.; Ono, M.; Kimura, H.; Kagawa, S.; Nishii, R.; Kawashima, H.; Saji, H. Fluorinated benzofuran derivatives for PET imaging of β-amyloid plaques in Alzheimer's disease brains. *ACS Med. Chem. Lett.* **2010**, *1*, 321−325.

(16) Ono, M.; Kawashima, H.; Nonaka, A.; Kawai, T.; Haratake, M.; Mori, H.; Kung, M. P.; Kung, H. F.; Saji, H.; Nakayama, M. Novel benzofuran derivatives for PET imaging of β-amyloid plaques in Alzheimer's disease brains. *J. Med. Chem.* **2006**, *49*, 2725−2730.

(17) Chandra, R.; Oya, S.; Kung, M. P.; Hou, C.; Jin, L. W.; Kung, H. F. New diphenylacetylenes as probes for positron emission tomographic imaging of amyloid plaques. *J. Med. Chem.* **2007**, *50*, 2415−2423.

(18) Stephenson, K. A.; Chandra, R.; Zhuang, Z. P.; Hou, C.; Oya, S.; Kung, M. P.; Kung, H. F. Fluoro-pegylated (FPEG) imaging agents targeting Aβ aggregates. *Bioconjug Chem* **2007**, *18*, 238−246.

(19) Wang, J.; Dickson, D. W.; Trojanowski, J. Q.; Lee, V. M. The levels of soluble versus insoluble brain Aβ distinguish Alzheimer's disease from normal and pathologic aging. *Exp. Neurol.* **1999**, *158*, 328−337.

(20) Khatoon, S.; Grundke-Iqbal, I.; Iqbal, K. Brain levels of microtubule-associated protein tau are elevated in Alzheimer's disease: A radioimmuno-slot-blot assay for nanograms of the protein. *J. Neurochem.* **1992**, *59*, 750−753.

ACS Chemical Neuroscience

Research Article

pubs.acs.org/acschemicalneuroscience

BODIPY-Based Molecular Probe for Imaging of Cerebral β-Amyloid Plaques

Masahiro Ono,* Hiroyuki Watanabe, Hiroyuki Kimura, and Hideo Saji

Department of Patho-Functional Bioanalysis, Graduate School of Pharmaceutical Sciences, Kyoto University, 46-29 Yoshida Shimoadachi-cho, Sakyo-ku, Kyoto 606-8501, Japan

Supporting Information

ABSTRACT: We designed and synthesized a BODIPY-based probe (BAP-1) for the imaging of β-amyloid plaques in the brain. In binding experiments in vitro, BAP-1 showed excellent affinity for synthetic Aβ aggregates. β-Amyloid plaques in Tg2576 mouse brain were clearly visualized with BAP-1. In addition, the labeling of β-amyloid plaques was demonstrated in vivo in Tg2576 mice. These results suggest BAP-1 to be a useful fluorescent probe for the optical imaging of cerebral β-amyloid plaques in patients with Alzheimer's disease.

KEYWORDS: *Alzheimer's disease, β-amyloid plaque, BODIPY, optical imaging*

The formation of β-amyloid (Aβ) plaques is a critical neurodegenerative change in Alzheimer's disease (AD).[1,2] Since the imaging of Aβ plaques in vivo may enable the presymptomatic diagnosis of AD, several imaging technologies including positron emission tomography (PET),[3−21] single photon emission computed tomography (SPECT),[22−24] magnetic resonance imaging,[25−28] and optical imaging[29−33] have been applied for this purpose. In particular, several PET probes have shown the feasibility of imaging Aβ plaques in AD brains. PET imaging is an established clinical modality that provides good sensitivity deep in tissue. However, it is limited by a time-consuming data acquisition process, exposure to radioactivity, the need for expensive equipment and highly skilled personnel, and a relatively poor spatial resolution.

Conversely, optical imaging with fluorescent probes is a relatively new modality that offers real-time, nonradioactive, and, depending on the technique, high-resolution imaging,[34] leading to a rapid, inexpensive, and nonradioactive drug screening system for AD. However, there have been fewer reports regarding the development of fluorescent probes than PET probes despite their significance, although AOI-987,[29] NIAD-4,[30] CRANAD-2,[32] ANCA-11,[35] and BMAOI[36] have been reported for the imaging of Aβ plaques.

Compounds containing a boron dipyrromethane (BODIPY) scaffold have widespread applications as dyes, fluorescent probes in biological systems, and materials for incorporation into electroluminescent devices.[37−40] Their broad utility is due to their high thermal and photochemical stability, chemical robustness, and tunable fluorescence properties. We have previously reported a dual SPECT/fluorescent probe based on the BODIPY scaffold, for the imaging of Aβ plaques in vivo.[41] Despite good affinity for synthetic Aβ(1−42) aggregates and the clear labeling of Aβ plaques in sections of the mouse brain, the BODIPY-based probe was not suitable for imaging in vivo due to its poor uptake into the brain. Two other papers have reported BODIPY-based probes targeting Aβ plaques.[42,43] However, these derivatives have not been applied to imaging in vivo perhaps due to their low brain uptake and short excitation/emission wavelength, though they showed high affinity for Aβ plaques in vitro. The findings of these previous studies suggested that additional structural changes may modify the properties of BODIPY derivatives to improve their suitability for imaging in vivo.

Many Aβ-imaging probes for PET applied in clinical trials possess a dimethylamino styryl group as a consensus structure as reported previously.[3,22,44−46] Then, in the present study, we designed and synthesized a new BODIPY-based Aβ probe (BAP-1) with a dimethyamino styryl group which plays an important role in binding to Aβ aggregates. BAP-1 belongs to a class of dyes that are collectively called molecular rotors, where the dimethyl-aniline is the donor, and the BODIPY unit is the acceptor.[47] This motif is typical of Aβ-imaging probes. Here, we report the in vitro and in vivo evaluation of BAP-1 as a new probe for the optical imaging of cerebral Aβ plaques.

■ RESULTS AND DISCUSSION

The target BODIPY derivative (BAP-1) was synthesized as shown in Scheme 1. Although the synthetic route for this compound has been reported,[37] we made some modifications. The key step in the formation of the BODIPY backbone (**3**) was accomplished by the condensation of pyrrole 2-carboxyaldehyde (**1**) and 2,4-dimethylpyrrole (**2**) at low temperature, followed by the addition of $BF_3{\cdot}OEt_2$ in a yield of 36.1%. Compound **4** (BAP-1) was successfully prepared by the condensation of **3** and 4-dimethyl-aminobenzaldehyde in the presence of piperidine and acetic acid (50.6% yield).

Received: January 18, 2012
Accepted: February 7, 2012
Published: February 17, 2012

Scheme 1. Synthetic Route for BAP-1[a]

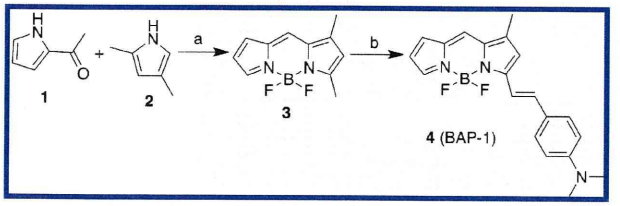

[a]Reagents: (a) $CHCl_3$, $POCl_3$, BF_3OEt_2, Et_3N; (b) toluene, 4-dimethylaminobenzaldehyde, piperidine, and AcOH.

First, we evaluated the fluorescent properties including absorption, excitation, emission wavelength, and quantum yield of BAP-1 in $CHCl_3$. BAP-1 exhibited absorption, excitation, and emission wavelengths of 604, 614, and 648 nm, respectively, with a high fluorescent quantum yield (46.8%) (Table 1). Although

Table 1. Fluorescence Characterization of BAP-1[a]

Abs (nm)	Ex (nm)	Em (nm)	quantum yield (%)
604	614	648	46.8

[a]Absorbance, fluorescence excitation and emission, and quantum yield of BAP-1 were determined with 10 μM of the compound in $CHCl_3$.

BAP-1 showed slightly shorter wavelengths of excitation/emission at 614/648 nm than are appropriate for optical imaging in vivo, its high quantum yield was expected to enable the imaging of Aβ plaques in shallow areas of the mouse brain.

Furthermore, when BAP-1 existed in a solution containing Aβ aggregates or bovine serum albumin (BSA), its fluorescent intensity increased with the concentration of the aggregates, indicating affinity for Aβ aggregates (Figure 1). However, we

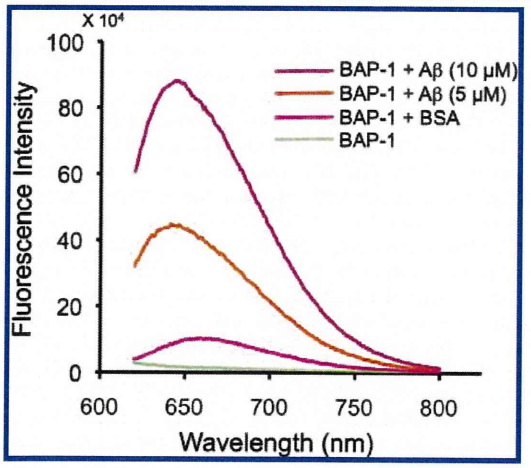

Figure 1. Fluorescence intensity of BAP-1 upon interaction with Aβ42 aggregates and BSA.

found no significant change in fluorescence during the incubation with BSA, indicating that there is little interaction between BAP-1 and BSA.

To quantify the affinity for Aβ aggregates, we measured the apparent binding constant (K_d) of BAP-1 by conducting a saturation assay (Figure 2). The fluorescent intensity of BAP-1 increased in a dose-dependent manner and was saturated at the higher concentration. Transformation of the saturation binding data to Scatchard plots provided linear plots, indicating that

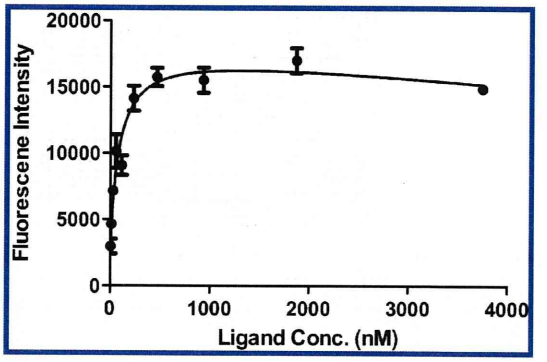

Figure 2. Plot of the fluorescence intensity (Em = 673 nm) as a function of the concentration of BAP-1 in the presence of Aβ42 aggregates (2.2 μM) in solutions.

BAP-1 has one binding site on Aβ aggregates. BAP-1 showed excellent affinity for Aβ aggregates at a K_d value of 44.1 nM.

To confirm the affinity of BAP-1 for Aβ plaques in the brain, neuropathological fluorescent staining with BAP-1 was carried out using brain sections from Tg2576 mice (Figure 3). Tg2576 mice have been specifically engineered to overproduce Aβ plaques in the brain[48] and frequently used to evaluate the specific binding of Aβ plaques in experiments in vitro and in vivo.[49−51] Many fluorescent spots were observed in the brain sections of Tg2576 mice (32-month-old, female) (Figure 3A), while no spots were observed in the wild-type mice (29-month-old, female) (Figure 3B). The staining pattern was consist with that observed with thioflavin S (Figure 3C), a dye commonly used to stain Aβ plaques,[52] indicating that BAP-1 shows specific binding to Aβ plaques in the mouse brain.

One important prerequisite for a probe for imaging of Aβ plaques in the brain is to penetrate the blood−brain barrier after an i.v. injection. Furthermore, the ideal amyloid-imaging agent should be rapidly washed out from normal brain tissue in addition to having a high brain uptake. Since normal brain tissue has no amyloid plaques to trap the agent, the washout should be fast, providing a higher signal-to-noise ratio in the AD brain. To test the uptake into and washout from the brain, we determined the fluorescent intensity in the brain after the injection of BAP-1 into a normal mouse. BAP-1 showed high initial brain uptake at 2 min postinjection, but the fluorescence that accumulated in the brain was rapidly eliminated, both of which are highly desirable properties for Aβ imaging probes (Figure 4).

To evaluate the potential of BAP-1 in living brain tissue, we carried out experiments ex vivo using a Tg2576 mouse (25-month-old male) and a wild-type mouse (25-month-old male) as an age-matched control. The fluorescence in whole brains removed at 1 h postinjection of BAP-1 was much higher in the Tg2576 mouse than wild-type mouse (Figure 5).

To further evaluate what the higher fluorescence in the Tg2576 mouse brain was derived from, we prepared frozen sections from both brains and observed them with a fluorescence microscope. The brain sections from the Tg2576 mouse showed distinctive staining of Aβ plaques by BAP-1 (Figure 6A), while those from the wild-type mouse showed no such staining (Figure 6B). The staining pattern in the brain sections from the Tg2576 mouse was consistent with that observed on immunohistochemical staining with an antibody specific for Aβ(1−42) (BC05) as shown by arrows in Figure 6C. The results suggest that BAP-1 penetrated the blood−brain